SUMMER COVARIABILITY OF SURFACE CLIMATE FOR RENEWABLE ENERGY ACROSS THE CONTIGUOUS UNITED STATES: ROLE OF THE NORTH ATLANTIC SUBTROPICAL HIGH

A Thesis

Presented to the Faculty of the Graduate School

of Cornell University

In Partial Fulfillment of the Requirements for the Degree of

Master of Science

by

Kenji Morinaka Doering

December 2019

ABSTRACT

This study examines the joint spatiotemporal variability of summertime climate linked to renewable energy sources (precipitation and streamflow, wind speeds, insolation) and energy demand drivers (temperature, relative humidity, and a heat index) across the contiguous United States (CONUS) between 1948 and 2015. Canonical correlation analysis is used to identify the primary modes of joint variability between wind speeds and precipitation and related patterns of the other hydrometeorological variables. The first two modes exhibit a pan-US dipole with lobes in the eastern and central CONUS. Composite analysis shows that these modes are directly related to the displacement of the western ridge of the North Atlantic subtropical high (NASH), suggesting that a single, large-scale feature of atmospheric circulation drives much of the large-scale climate co-variability related to summertime renewable energy supply and demand across the CONUS. The impacts of this climate feature on the U.S. energy system are shown more directly by examining changes in surface climate variables at existing and potential sites of renewable energy infrastructure and locations of high energy demand. Finally, different phases of the NASH are related to concurrent and lagged modes of oceanic and atmospheric climate variability in the Pacific and Atlantic basins, with results suggesting that springtime climate over both oceans may provide some potential to predict summer variability in the NASH and its associated surface climate. The implications of these findings for the impacts of climate variability and change on integrated renewable energy systems over the CONUS are discussed.

BIOGRAPHICAL SKETCH

Kenji Doering was born in Middletown, Connecticut. Following the completion of schoolwork at La Cueva High School in Albuquerque, New Mexico in 2010, Kenji enrolled at the University of Washington in Seattle, Washington. He graduated from the University of Washington in 2014 with a Bachelor of Science degree in Biophysics with Minors in Mathematics and Chemistry. Following two years of work in a Biophysics laboratory at the University of Washington, he entered the Biological and Environmental Engineering graduate program at Cornell University in 2016.

Dedicated to my family, Lincoln, Toki, Tofu, and Yoshi

ACKNOWLEDGMENTS

I would like to acknowledge my advisors Scott Steinschneider and Lindsay Anderson for funding and mentoring me through this work, as well as my peers for supporting me outside of work.

TABLE OF CONTENTS

1. Introduction

Continued growth in the U.S. renewable energy sector is critical to reduce national greenhouse gas emissions under growing population and energy demands. In 2017, hydropower, wind energy, and solar energy contributed 7.5%, 6.3%, and 1.3% of total U.S. generation, respectively. High growth in wind (8.65%/year) and solar (42%/year) over the last 5 years has been driven by declines in unit cost from technological advances, economies of scale in production, and federal and state tax incentives (EIA 2017). As the penetration of non-dispatchable renewables into the national energy portfolio increases, variability in renewable energy sources (rainfall and streamflow, surface wind speeds, insolation) as well as climate drivers of energy demand (temperature and relative humidity) pose major challenges to the stability and reliability of the energy system (Zahedi 2011; Ronalds et al. 2014).

Much attention has been paid to shortages and intermittency in renewables like wind speeds and insolation on short timescales (sub-hourly to daily). Gusts, squalls, stillings, and local cloud cover cause uncontrolled fluctuations in wind and solar power output on these time scales, reducing the compatibility of these power sources with the instantaneous supply-demand energy balance requirements of the electricity grid (Zahedi 2011; Chang et al. 2013; Sims 2014; Cardell and Anderson 2015). A host of solutions has been proposed to manage fluctuations on these time scales (Castronuovo and Lopes 2004; Fertig et al. 2010; Vasquez et al. 2010; Dunn et al. 2011; Kempton 2012; Hirth 2016).

Presently, the impacts of long-term (inter-annual) variability in the climate system on renewable generation are best understood for hydropower systems. In the U.S. and globally, there has been substantial progress in our understanding of historic hydroclimate variability (Trenberth et al. 1988; Piechota and Dracup 1996; Barlow et al. 2001; Goodrich 2007; Fernández-González 2012; García-Ortega et al. 2014), and dynamic climate modeling has enabled attribution studies to link droughts and pluvials on multi-annual timescales with large-scale, quasi-oscillatory patterns of oceanic and atmospheric circulation (Schubert et al. 2009; Wang et al. 2010; Kushnir et al. 2010; Seager and Hoerling 2014). When these longer-term oscillations lead to prolonged drought, hydropower generation can fall substantially, requiring alternative generation sources to compensate (Miles et al. 2000; Cherry et al. 2005; Nobre et al. 2016).

Recently, research has shown that wind shortages can also occur on longer timescales and manifest through climate anomalies such as persistent high-pressure systems that block low-level circulation (Abhishek et al. 2010; Li et al. 2010; Bichet et al. 2012; Watson 2014; Hamlington et al. 2015; Kirchner-Bossi et al. 2015; Yu et al. 2015). The 2015 wind drought in the Western U.S provides a timely example, where wind speeds over parts of California fell as much as 20% below average and wind power, cubic with speed, fell even further (DNV-GL 2016). Importantly, the California wind drought occurred during the fourth year of the worst hydrologic drought in state history, causing concurrent shortfalls in two major sources of renewable power output (EIA 2015). The concurrence of wind and water droughts in 2015 was not coincidental, but rather was linked by the same persistent, high-pressure system that blocked winds and rain over

the Western U.S. coast (Swain et al. 2016). This system was also observed in previous years of the 2011-2016 California drought (Wang et al. 2014; Seager et al. 2015). Similarly, linkages have also been found between variations in insolation over the southwest US and other large-scale teleconnection patterns like the El Niño Southern Oscillation (ENSO; Mohammadi and Goudarzi 2018b), which is known to influence precipitation and temperature patterns in that region (Ropelewski and Halpert 1986). These studies suggest that large-scale atmospheric circulation organizes variations in surface climate at seasonal to inter-annual timescales related to renewable energy supply and demand (e.g., rainfall and streamflow, wind speeds, insolation, temperature, and relative humidity). This joint structure can manifest as either positive or negative anomalies among these hydrometeorological variables and could extend over regional or continental spatial scales, depending on the season and predominant circulation regimes at play.

The exploration of long-term joint variability of renewable energy supply and sources of demand and the dynamical processes behind them have only very recently been considered, often with a focus on insolation and wind speeds (Widén 2011; Santos-Alamillos et al. 2012; Jerez and Trigo 2013; Monforti et al. 2014; Bett and Thorton 2016) or wind speeds and temperature (Thornton et al. 2017; Bloomfield et al. 2018). We were only able to identify a few studies that investigated the long-term (seasonal to inter-annual) co-variability of three or more hydrometeorological variables related to renewable energy supply and demand (Ely et al. 2013; Jerez et al. 2013; Mohammadi and Goudarzi 2018a). A recent review found a similar gap in the literature (Engeland et

al. 2017). Furthermore, the majority of previous work has focused on Europe and the impacts of the North Atlantic Oscillation (NAO) in the cold season. An exception is the analysis of Mohammadi and Gourdarzi (2018a), which focused on California and cold season teleconnections to ENSO. Notably however, a similar analysis for the contiguous United States (CONUS) is still missing, particularly for the summer season when energy usage has historically been most intense (Bartos et al. 2016; EIA 2017).

There is a growing body of work showing that summer climate over North America is strongly influenced by the position and strength of the North Atlantic subtropical high (NASH). The NASH is a semi-permanent anticyclone established under the descending branch of the Hadley cell (Davis et al. 1997). In the summer, the NASH spans most of the subtropical North Atlantic Ocean, and clockwise circulation around its western ridge induces low-level southwesterly flow that transports warm, moist air from the Gulf of Mexico over the eastern U.S. (Gimeno et al. 2010; see Fig. 1). Importantly, the orientation and westward extent of the NASH western ridge largely determine precipitation patterns across much of the eastern U.S., particularly in the southeast and central CONUS region (Diem 2006; Li et al. 2011; Li et al. 2012a; Li et al. 2017). Past work also suggests that the position and strength of the NASH can be influenced by global modes of oceanic and atmospheric variability. For instance, Li et al. (2012a) found links between certain modes of the NASH and the Pacific Decadal Oscillation (PDO), while Wang et al. (2010) found that both Pacific and Atlantic sea surface temperatures (SSTs) can influence diabatic heating anomalies over the Gulf of Mexico, forcing low-level, anomalous cyclonic flow that influences NASH strength and its

westward extent. These results suggest that modes of Pacific and Atlantic SST anomalies like the PDO, Atlantic Multidecadal Oscillation (AMO), and North Atlantic Tripole (NAT) could inform seasonal forecasts of the NASH and by extension related surface climate linked to renewable energy supply and demand. Furthermore, recent work has projected that the western ridge of the NASH will extend westward in the summer under anthropogenic climate change (Li et al. 2012b; Thibeault and Seth 2014; Thibeault and Seth 2015; Ryu and Hayhoe 2017), with important implications for the sustainability of renewable energy systems.

Despite the potential importance of the NASH as a major driver of renewable energy supply and demand in the summer across the CONUS, the link between the NASH and co-variability of summertime hydrometeorological variables relevant to renewable energy has been underexplored, including the potential for seasonal forecasting and long-term trends linked to climate change. In the context of this research gap, this study contributes the first investigation of co-variability of summertime (June-August, JJA) sources of renewable energy supply (precipitation and streamflow, surface wind speeds, insolation) and drivers of demand (temperature, relative humidity, and a heat index) across the entire CONUS between 1948-2015, along with an assessment of large-scale climatological drivers. In particular, we focus on the position of the western ridge of the NASH and its influence on these patterns of co-variability. We explore inter-annual variability and long-term trends in the location of the NASH western ridge to determine its link to global patterns of oceanic and atmospheric variability, the potential for seasonal forecasting, and whether there are significant trends in the climatology of the

NASH. We conclude with a discussion of the implications of the results for renewable power systems over the CONUS.

2. Data

Gridded monthly surface wind speed, relative humidity, and 850 hPa geopotential height at a 2.5°x 2.5° resolution were obtained over the CONUS from the National Center of Environmental Prediction/National Center of Atmospheric Research (NCEP/NCAR) Reanalysis Project Phase I (Kalnay et al. 1996) and averaged over JJA for the years 1948-2015. The NCEP/NCAR dataset provides a relatively long reanalysis-based record of surface winds (68 years), supporting the estimation of robust long-term patterns of co-variability with other climate fields. We also collect wind speed data from the ERA-20C reanalysis at a 1.25°x 1.25° resolution (Poli et al. 2016) and ERA-Interim reanalysis at a 0.75°x 0.75° resolution (Dee et al. 2011) to verify and support the results of the analysis based on the NCEP reanalysis data.

Gauge-based, gridded precipitation data at a 0.25°x0.25° resolution for the CONUS were acquired from the National Oceanic and Atmospheric Administration (NOAA) Climate Prediction Center (CPC), as part of the Unified Precipitation Project (Chen et al. 2008; Xie et al. 2007; Xie et al. 2008). Summer totals of daily precipitation were used between the years 1948-2015. Similar to wind speeds, a separate precipitation dataset at a 0.25°x0.25° spatial resolution (Livneh et al. 2013) was also collected and averaged over each summer to verify patterns of co-variation identified using the CPC precipitation data.

Gridded observation-based monthly average temperature from 1948-2015 at a 0.5°x0.5° resolution was acquired from NOAA CPC based on the Global Historical Climatology Network version 2 and the Climate Anomaly Monitoring System (GHCN+CAMS) datasets (Fan and van den Dool 2008).

Gridded incident shortwave radiation was acquired from the NASA/GEWEX Surface Radiation Budget (SRB) monthly data set between 1984-2007 at a 1°x1° resolution and averaged across the summer season. The SRB data set includes cloud and surface properties from the International Satellite Cloud Climatology Project, which uses visible and infrared radiance data as model inputs (SRB Science Team 2010).

Daily streamflow data was acquired from the United States Geological Survey (USGS) Geospatial Attributes of Gages for Evaluating Streamflow II (GAGES-II) dataset (Falcone et al. 2010). Reference gages with low anthropogenic impact and at least 40 years of data between 1948-2015 were selected for the analysis.

A heat index (HI) was calculated for the CONUS using NCEP/NCAR relative humidity and GHCN+CAMS temperature and functions detailed by NOAA (http://www.wpc.ncep.noaa.gov/html/heatindex_equation.shtml). HI characterizes the heat stress one experiences and is more directly linked to energy demand for cooling. The HI is at the same spatial and temporal resolution as the temperature dataset. Relative humidity was interpolated to this resolution using a bilinear interpolation.

Monthly SST data was acquired from 1948-2015 on a 1°x1° resolution from the NOAA Extended Reconstructed Sea Surface Temperature V4 Dataset (Huang et al. 2014; Liu et al. 2014; Huang et al. 2015).

Oceanic indices for the ENSO (Niño 3.4; Trenberth 1997), the PDO (Mantua et al. 1997), and the AMO (Enfield et al. 2001), as well as atmospheric indices for the Pacific/North American pattern (PNA) and the NAO (Barnston and Livezey 1987), were acquired from NOAA's Earth System Research Laboratory - Physical Science Division (https://www.esrl.noaa.gov/psd/data/climateindices/list/). Following Steinschneider and Brown (2011), we also develop an index representing the North Atlantic Tripole ($NAT = SST_1 - SST_2 + SST_3$) by adding together averaged SSTs in three regions (Region 1: 43.1°N-58.2°N × 33.4°W-64°W; Region 2: 22.1°N-43.1°N × 33.4°W-64°W; Region 3: 2°N-22°N × 33.4°W-64°W).

All climate and hydrologic data above were averaged over the summer (JJA). All datasets used in this study are summarized in Table 1.

Dataset	Variable(s)	Spatial Resolution	Temporal Extent Used
NCEP/NCAR	Wind Speed, Relative Humidity, 850 hPa Geopotential Height	2.5°x2.5°	1948-2015
ERA-20C	Wind Speed	1.25°x 1.25°	1948-2010
ERA-Interim	Wind Speed	0.75°x0.75°	1979-2015
NOAA CPC	Precipitation	0.25°x0.25°	1948-2015
Livneh et al.	Precipitation	0.25°x0.25°	1948-2015
NOAA CPC GHCN+CAMS	Temperature	0.5°x0.5°	1948-2015
NASA/GEWEX SRB	Insolation	1°x1°	1984-2007
USGS GAGES-II	Streamflow	N/A	1948-2015
NOAA	Sea Surface Temperature	2°x2°	1948-2015

Table 1. *Summary of the datasets used in this study.*

Finally, to more directly relate renewable energy infrastructure to climate patterns, we collected the locations of existing hydropower facilities and non-power dams that have potential to have turbines installed (Hadjerioua et al. 2012), wind turbines (Draxl et al. 2015), solar power plants (EIA 2018), and high-population cities (US Census Bureau 2015) across the CONUS.

3. Methods

3.1. Modes of Joint Variability

Canonical correlation analysis (CCA; Wilks 2006) was used to extract the major modes of joint variability between surface wind and precipitation fields from 1948-2015. CCA identifies loading vectors (a,b) that maximize the correlation between canonical variates

u and *v*, which are linear combinations of JJA average, gridded wind speeds (*w*) and precipitation (*p*) across the CONUS, respectively:

$$u = wa^T; v = pb^T \quad \text{(Eq. 1)}$$

$$\max_{a,b} cor(u, v) \quad \text{(Eq. 2)}$$

The loading vectors identify the most prominent, concurrent spatial patterns in summertime wind speeds and precipitation, while the canonical variates represent the temporal variability of those patterns. To identify the canonical vectors and variates, CCA performs an eigendecomposition of a matrix formed by the product of covariance matrices of the two data fields. However, the annual data (1 value per summer season) only spans a 68-year period (1948-2015), and so there are substantially less observations than grid cells for both the wind speed and precipitation fields. The covariance matrices are singular in such an underdetermined system, impeding the eigendecomposition in CCA. Therefore, we use a regularized version of CCA (Vinod 1976; Leurgans et al. 1993; Ho et al. 2016) to stabilize the inversion, which has the effect of smoothing the resulting spatial patterns. Different regularization constants for the precipitation and wind speed data are selected via a cross-validation procedure. We focus on the first two modes of variability, represented by pairs of canonical variates ((u_1, v_1) and (u_2, v_2)), and summarize the temporal variability of these patterns using simple averages (CC1 = (u_1 + v_1)/2 and CC2 = (u_2 + v_2)/2) because the correlation between pairs of canonical variates is very high (>0.99 for both (u_1, v_1) and (u_2, v_2)). Regularized CCA is performed

in the R programming language (version 3.3.1) using the rcc() function from the package “CCA” (González et al. 2008).

CCA is designed to identify joint patterns between two climate fields. To consistently present how climate variables for renewable energy supply (precipitation and streamflow, wind speeds, insolation) and drivers of demand (temperature, relative humidity, and HI) co-vary with the patterns identified above, we correlate these data on a grid-cell by grid-cell basis with both CC1 and CC2 (gage by gage for streamflow), and then map the correlation coefficients across the CONUS. Statistical significance at the 5% level is tested using two-tailed t-tests for each correlation value in each grid cell. We also confirm the significance of the patterns using a false discovery rate for field significance. The patterns identified using NCEP reanalysis surface wind speeds and CPC precipitation data are verified by also applying regularized CCA to surface wind speeds from the ERA-20C reanalysis and precipitation from Livneh et al. (2013), and also by applying CCA to different pairs of climate fields (i.e., the HI paired separately with precipitation and wind speeds). This pairwise approach to verification was chosen in favor of conducting CCA over all hydrometeorological fields simultaneously because 1) the partitioning of variables into separate matrices would have been arbitrary but would have influenced the final identified patterns, and 2) CCA over all hydrometeorological fields would have required a stronger regularization due to the higher ratio of variables to observations. In addition, we note that pairwise CCA was not attempted with streamflow or insolation because they did not have sufficient, continuous data over the 1948-2015 period to support robust pattern recognition, and

streamflow gages are unevenly distributed across the CONUS, which would unduly place more weight on certain regions in the CCA.

3.2. Relations to the North Atlantic Subtropical High

In order to examine the relation to the NASH, we follow Li et al. (2011, 2012a) and characterize the western ridge of the NASH as the intersection between the 1560 geopotential meter (gpm) isohypse of seasonally averaged 850 hPa geopotential heights and the isotach at which the zonal component of seasonally averaged 850 hPa wind velocity is zero. The position of the western ridge of the NASH can then be categorized into quadrants based on its position relative to the mean climatological position (29°N, 85°W; Fig. 1a), or more simply based on its longitudinal location (Fig. 1b). The quadrants are used to group the position of the NASH western ridge into four typologies: northwest (NW; Fig. 1c), northeast (NE; Fig. 1d), southwest (SW; Fig. 1e), and southeast (SE; Fig. 1f) ridging. Figure 1(c-f) shows the NASH orientation, 850 hPa wind velocities, and precipitation anomalies under these typologies. Extending the work of Li et al. (2012a), we composite all climate fields (precipitation, streamflow, wind speed, insolation, temperature, humidity, and the HI) for each NASH typology and compare the resulting patterns to those identified through CCA. We also compare the time series of discrete NASH typologies to CC1 and CC2 using multinomial logistic regression (model structure described later). This approach will help determine the degree to which the NASH accounts for the major modes of joint variability across the primary climate fields responsible for renewable energy supply and demand across the CONUS region. To assess the significance of the composite maps for the NASH quadrants, we utilize a

bootstrapping method. We generate composites from *n* randomly sampled years from the entire record 1000 times, where *n* is the number of years that are within a given quadrant of the NASH being tested. If the actual composite value for a particular grid cell and NASH quadrant fall outside of the 95% confidence interval for the 1000 bootstrapped composites, the value is considered significant. A Mann-Kendall test is used to assess the monotonic trend of the longitudinal location of the NASH western ridge in order to examine whether the climatology of this dynamical atmospheric feature may be changing in response to anthropogenic climate change (Mann 1945). This analysis updates a related trend analysis conducted by Li et al. (2012a) on data from 1948-1977 and 1977-2007 with data that extends to 2015 (see Fig. 1a).

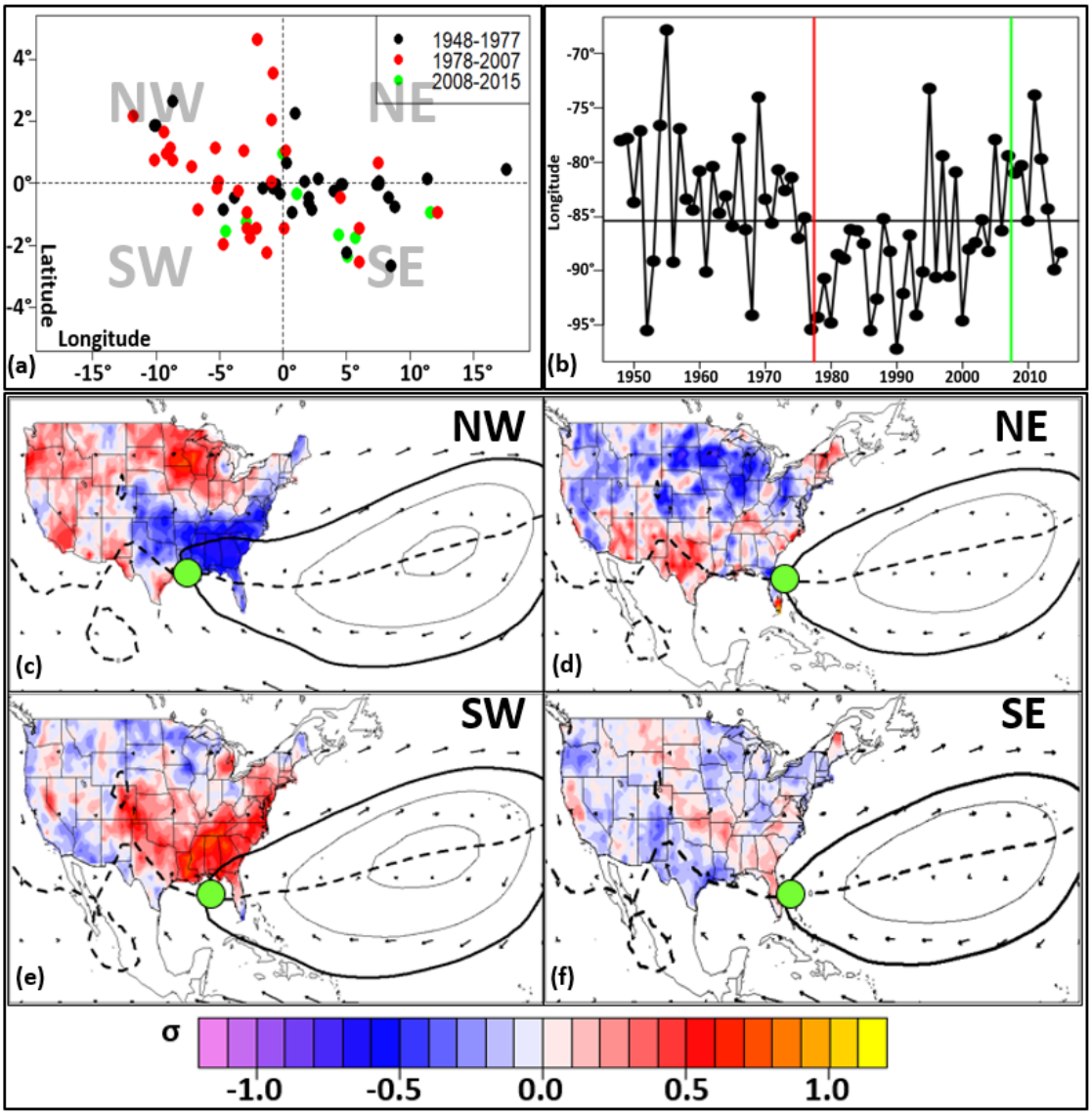

Figure 1. *(a) Location of the western ridge of the NASH relative to its climatological mean for 1948-1977 (black), 1978-2007 (red), and 2007-2015 (green). (b) Longitudinal position of the western ridge of the NASH from 1948-2015. The red and green lines are the years sectioned from panel a. Map of the NASH under the (c) NW, (d) NE, (e) SW and (f) SE typologies. Average 850 hPa geopotential heights for the summer season (solid contours; 20 gpm width) are shown with the 1560 gpm isohypse highlighted (bold contour). The western ridge of the NASH (green dot) is located at the intersection of the 1560 gpm isohypse and the isohypse of zero zonal winds (dashed line). Wind velocity at 850 hPa (vector field) and precipitation anomalies (shaded) are also shown. All data are averaged for years when the NASH western ridge is in each typology and shown as standard anomalies from the climatological mean.*

3.3. Impacts on Renewable Energy Supply and Demand

The potential impacts of the NASH on energy systems is explored by examining shifts in the distribution of relevant surface climate variables at locations of renewable energy infrastructure and sites of high demand during different orientations of the NASH western ridge. We show the location of existing and potential hydropower facilities (Hadjerioua et al. 2012), wind turbines (Draxl et al. 2015), solar power plants (EIA 2018), and high-population cities (US Census Bureau 2010), superimposed on climate patterns under two typologies (NW, SW) of NASH ridging. We also show the distribution of changes in precipitation, wind power (cubic of wind speed interpolated to 80 m hub height), insolation, and the HI in three sub-regions (Southeast, southern Great Plains, Midwest) under the NW and SW ridging typologies as compared to climatology. This analysis reveals how surface climate shifts under variability in the NASH directly impacts large-scale renewable energy supply and demand across the CONUS. While we only show results for two typologies for brevity, the analysis can be extended to the other typologies.

3.4. Large Scale Teleconnections

We end the analysis by examining summertime teleconnections between the NASH and global-scale modes of climate variability. We first composite concurrent (JJA) and lagged (March-May, MAM) SSTs for each of the four phases of the NASH western ridge to determine if there is any predictability in the ridge orientation and associated surface climate linked to oceanic forcing. Statistical significance for composite maps is assessed using bootstrapping, as described earlier. Based on the SST patterns identified

in the composites, we use multinomial regression to assess whether the position of the NASH western ridge has any concurrent or lagged association with oceanic indices for the ENSO (Niño 3.4), PDO, NAT, and AMO, as well as atmospheric indices for the PNA and NAO, for the JJA and MAM seasons. In this model, the probability of each state *k* of the NASH western ridge at year *t* is related to the teleconnection indices through a log-linear model:

$$\log P(NASH_t = k) = \boldsymbol{\beta}_k \boldsymbol{X}_t - \log Z \quad (3)$$

Here, $\boldsymbol{\beta}_k$ is a vector of regression coefficients unique to the kth state of the NASH western ridge, $\boldsymbol{X}_t$ is a vector of indices at time *t* (either MAM or JJA indices), and Z is a normalization term to ensure that the set of probabilities sum to one. Because of this summation constraint, only K-1=3 of the K=4 NASH states can have unique regression coefficients. We report regression results for the NW, NE, and SW ridging typologies, and use SE ridging as the pivot state (i.e., no regression coefficients are presented) because results show the response of surface climate under this state is least anomalous across the CONUS. To avoid issues of multicollinearity, the above model is developed separately for atmospheric and oceanic indices, because they often represent different manifestations of the same coupled mode of climate variability and are therefore highly correlated.

4. Results

4.1. Modes of joint surface climate variability linked to renewable energy

Pearson correlation coefficients between CC1 (Fig. 2a) and CC2 (Fig. 2b) and time series of CPC precipitation, streamflow, NCEP/NCAR reanalysis wind speed, insolation, relative humidity, temperature, and HI for each grid cell (reference stream gage) are shown in Figure 2c-p. The spatial patterns of correlation convey the structured organization in surface climate that emerges under the first two modes of joint variability between precipitation and wind speeds, as determined by CCA.

Several insights emerge from Figure 2. Under the first CCA pattern, all of the climate fields exhibit an east-west CONUS-wide dipole. When precipitation is anomalously high in the east and particularly in the Southeast, it is anomalously low in the Pacific Northwest and the northern extent of the central plains, and vice versa (Fig. 2c). As one would expect, the streamflow patterns under CC1 mirror those for precipitation (Fig. 2d), albeit to a lesser extent and significance due to the moderating effects of antecedent conditions on discharge and the weaker connection between summertime precipitation and streamflow in drier regions of the CONUS. Wind speeds exhibit a similar dipole but with a more eastward orientation, with stronger southerly flow over the central plains and anomalous northerly flow off the southeastern U.S. coastline (Fig. 2e). The pattern of insolation anomalies more closely tracks the east-to-northwest orientation seen for precipitation (Fig. 2f). For HI, the dipole pattern is entirely zonal, and is primarily driven by similar changes in temperature that overwhelm opposing shifts in relative humidity (Fig. 2k-m). In large part, the precipitation, streamflow, insolation,

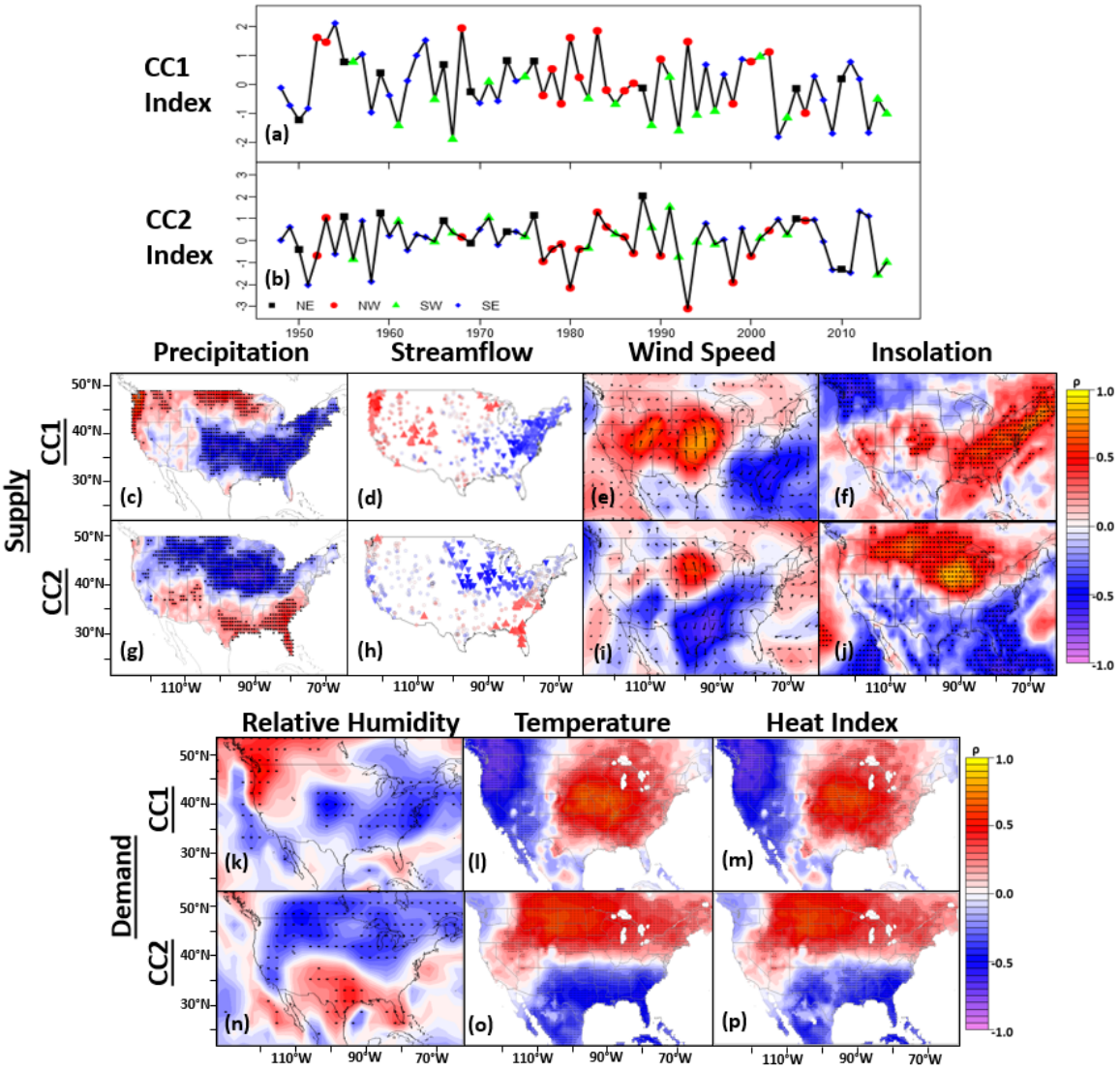

Figure 2. *Results of the Canonical correlation analysis. a,b) Time series of CC1 and CC2. NASH typologies for each year are marked. Correlations between CC1 and CC2 and renewable energy supply side (c-j) and demand side (k-p) climate variables. Statistical significance at the 95% level is shown by stippling (precipitation, insolation, relative humidity, temperature, heat index), triangles (streamflow) or the presence of wind vectors (wind speed). Local variance explained is given by the square of the local correlation coefficient.*

temperature, relative humidity, and HI patterns are physically consistent (lower levels of insolation and cooler temperatures accompany more humidity, rain, and cloudy skies) and are driven by the dipole in large-scale wind fields, which either direct Gulf of

Mexico moisture and cloud cover over the eastern U.S. coastline or further up the center of the CONUS region with the potential to curl towards the northwest (Smith and Baeck 2017).

Similar to CC1, the patterns under CC2 also exhibit CONUS-wide dipoles in all climate fields, but with a north-south orientation. For precipitation and streamflow, the pattern is strongest near Iowa, with a weaker southerly component (Fig. 2g,h). Wind speeds under CC2 are more spatially concentrated over the CONUS compared to CC1, with opposing lobes over the southern and northern plains (Fig. 2i). Similar to CC1, the insolation pattern under CC2 tracks that of precipitation closely, highlighting the link between rainfall and cloudy skies (Fig. 2j). Also similar to CC1, the HI dipole pattern under CC2 is driven by temperature, which overwhelms opposite variations in relative humidity (Fig. 2n-p).

Similar results are achieved when the analysis is repeated using gage-based precipitation from Livneh et al. (2013) and ERA-20C-based wind speed data, although the order of the canonical covariates is reversed (Fig. 3a-h). In addition, we assess the sensitivity of the analysis to alternative pairs of hydrometeorological variables used in the CCA, including CPC precipitation and HI (Fig. 3i-p) and NCEP/NCAR wind speeds and HI (Fig. 3q-x). We find that each combination of variables results in very similar patterns

to those in Figure 2. There are some small differences, and the first two modes of variability switch order under certain pairings. Overall though, the relationships do not

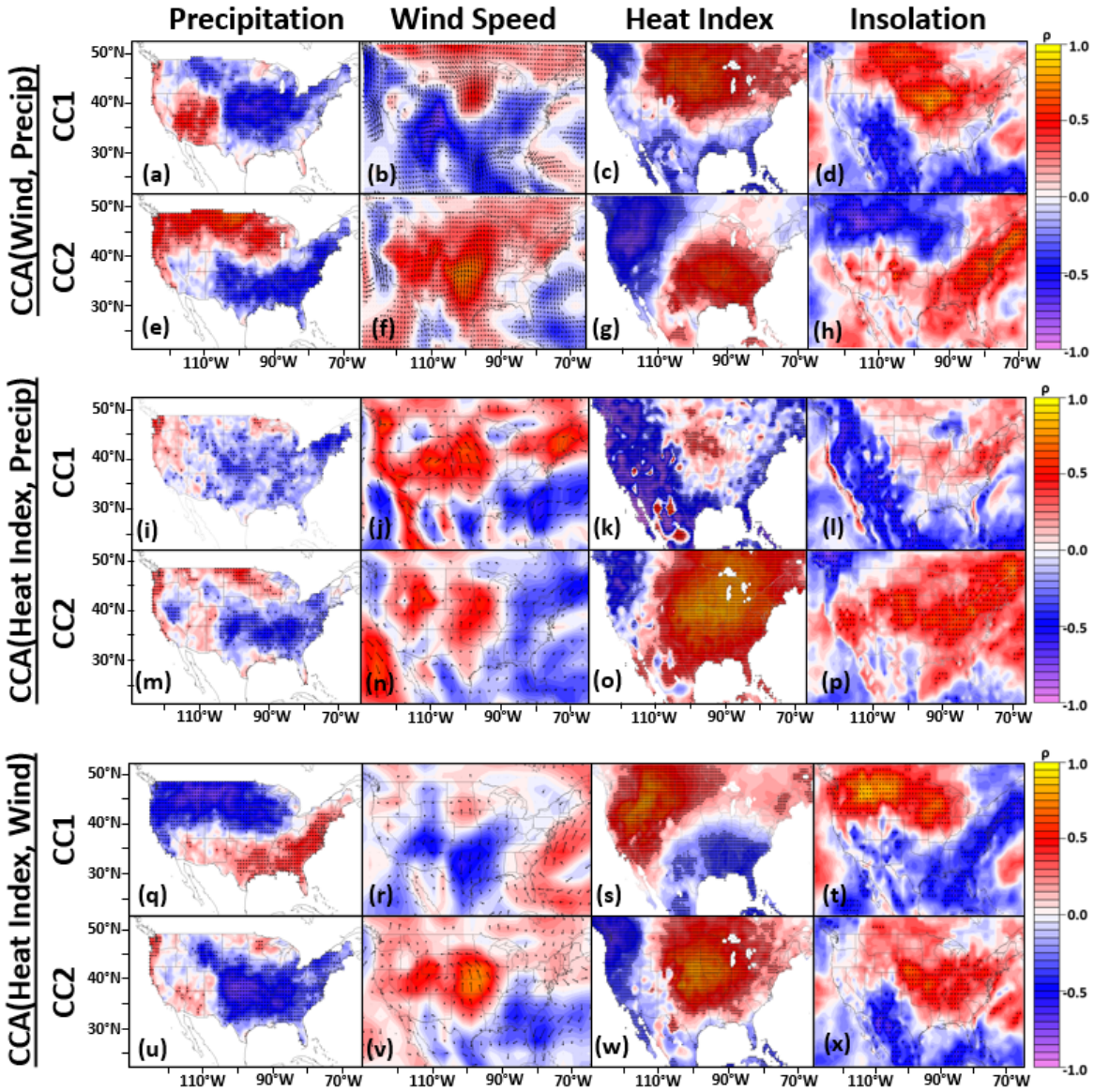

Figure 3 *The correlation of precipitation, wind speed, the heat index, and insolation to CC1 and CC2 based on CCA conducted with wind speed (ERA20C) and precipitation (Livneh) (a-h), HI and precipitation (CPC) (i-p), and HI and wind speed (NCEP/NCAR) (q-x).*

change substantially, indicating that the patterns in Figure 2 are reliable and not overly sensitive to the selected datasets or variables used in the analysis.

4.2. North Atlantic Subtropical High

The patterns identified above in Figures 2 and 3 clearly demonstrate cohesion of surface climate features relevant to renewable energy production and demand across the CONUS, but the associated large-scale atmospheric circulation that is linked with these patterns remains unclear. This is revealed through correlation maps between CC1 and CC2 (from Fig. 2) and 850 hPa geopotential height anomalies across the North American sector (Fig. 4). These maps show that CC1 is associated with a pan-North American wave train that includes opposing height anomalies off the eastern U.S. coast and south of the Great Lakes, while CC2 is associated with lobes of anomalous

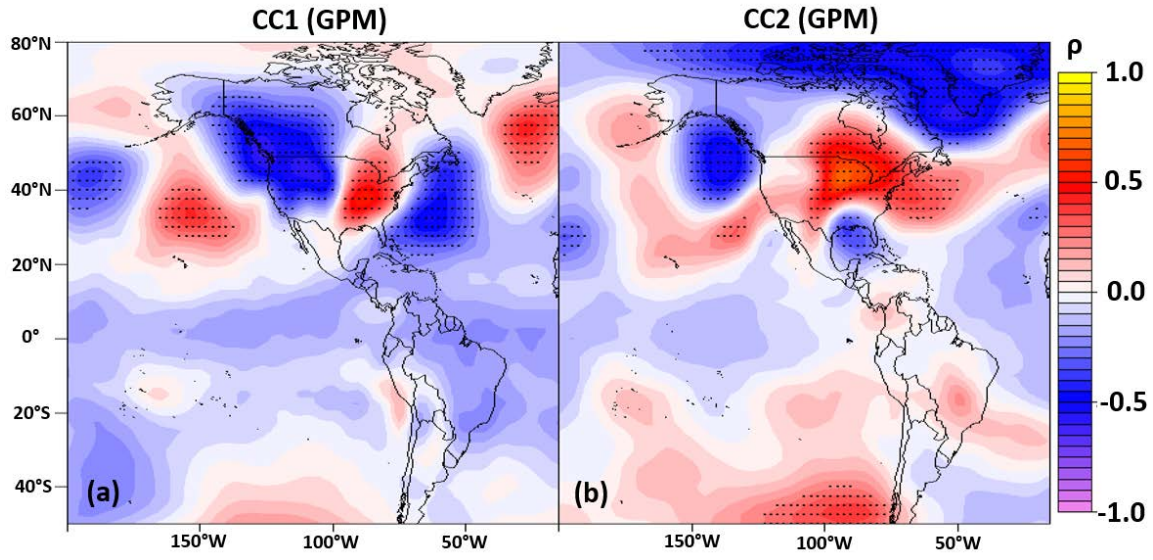

Figure 4. *Maps of (a) CC1 and (b) CC2 correlated to JJA average 850 hPa geopotential height*.

geopotential height over the Great Lakes and Gulf Coast. These results are very similar to composites of 850 hPa geopotential height anomalies under different typologies of the NASH western ridge orientation, as shown by Li et al. (2012a). Using a multinomial

regression, CC1 and CC2 also significantly relate to the temporal variability of NASH typologies (likelihood ratio test, p=0.00147).

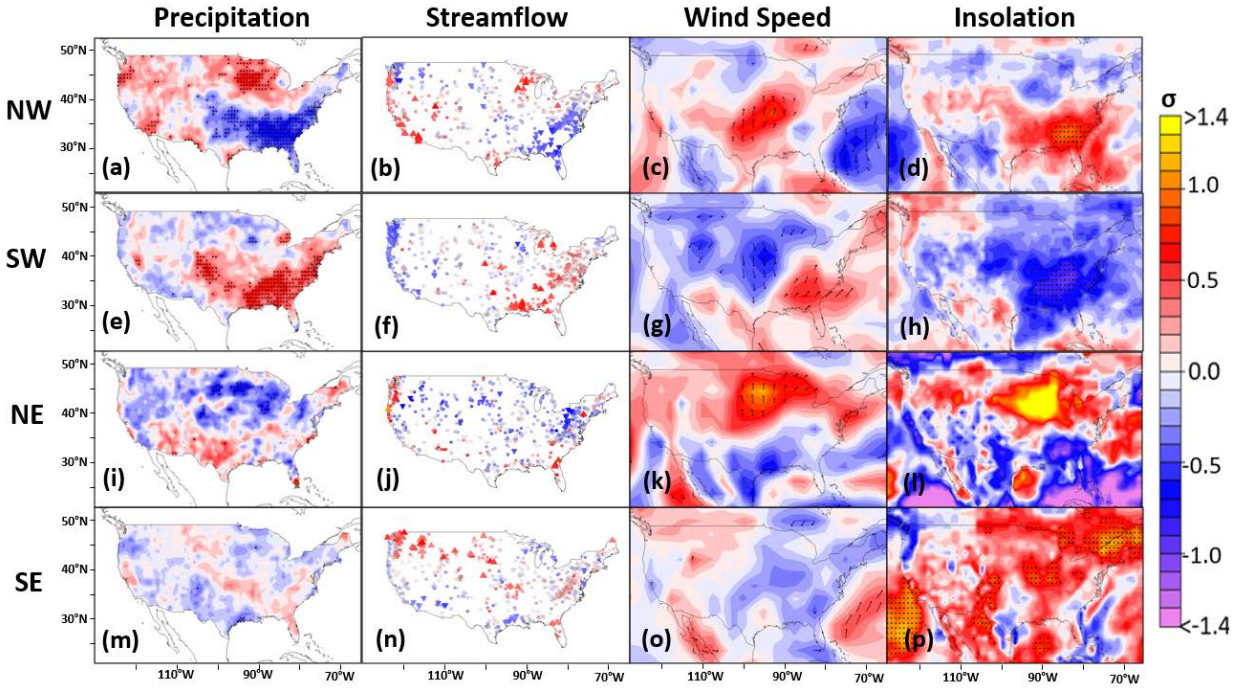

Figure 5. *Associations of renewable energy supply side climate variables with the location of the western ridge of the NASH. Composites of climate anomalies (in standard deviations from the mean) under different NASH western ridge typologies for NW (a-d), SW (e-h), NE (i-l), and SE (m-p) ridging. Statistical significance at the 95% level is shown by stippling (precipitation, insolation), triangles (streamflow) or the presence of wind vectors (wind speed).*

To better see the relationship between the NASH and both CC1 and CC2, we examine composites of precipitation, streamflow, wind speeds, and insolation (Fig. 5), as well as relative humidity, temperature, and HI (Fig. 6), during years of NW, SW, NE, and SE ridging. Many similarities can be seen between the maps associated with the CCA modes (Fig. 2,3) and the composite analysis over different NASH western ridge typologies (Fig. 5,6). For instance, surface climate anomalies under NW and SW typologies (Fig. 5a-h, and Fig. 6a-f) strongly mirror the two opposing manifestations of

the dipole patterns identified for CC1, particularly in the Eastern US. Under SW ridging, precipitation and streamflow increase in the southeast U.S. and decrease in the northern plains (Fig.5e,f), with the opposite pattern seen for NW ridging (Fig. 5a,b). The effects for streamflow are strongest in wet regions (e.g., the Southeast) where precipitation has the largest impact on summertime streamflow. Similarly, wind speeds increase (decrease) in the central plains and decrease (increase) in the Southeast and off the eastern US coast under NW (SW) ridging (Fig. 5c,g). Here, though, there are some asymmetries across the two typologies, including the southeast wind speed anomaly that occurs further east during NW compared to SW ridging. NW and SW insolation patterns also resemble the CC1 pattern, but less strongly, with the clearest resemblance observed in the southeast US (Fig. 5d,h). Both temperature and HI under the SW and NW typologies also exhibit near identical (but opposing) anomaly patterns similar to that seen under CC1, while relative humidity exhibits an opposing pattern to temperature, but varies less under the NW and SW phases of the NASH (Fig. 6a-f). Overall, the patterns identified under CC1 are clearly active during summers when the western ridge of the NASH is west of its mean climatological position, with the dipoles in CC1 associated with a NW or SW orientation of the ridge. This suggests that the position and orientation of the NASH drives a major pattern of co-variability in surface climate related to summertime renewable energy supply and demand across the CONUS.

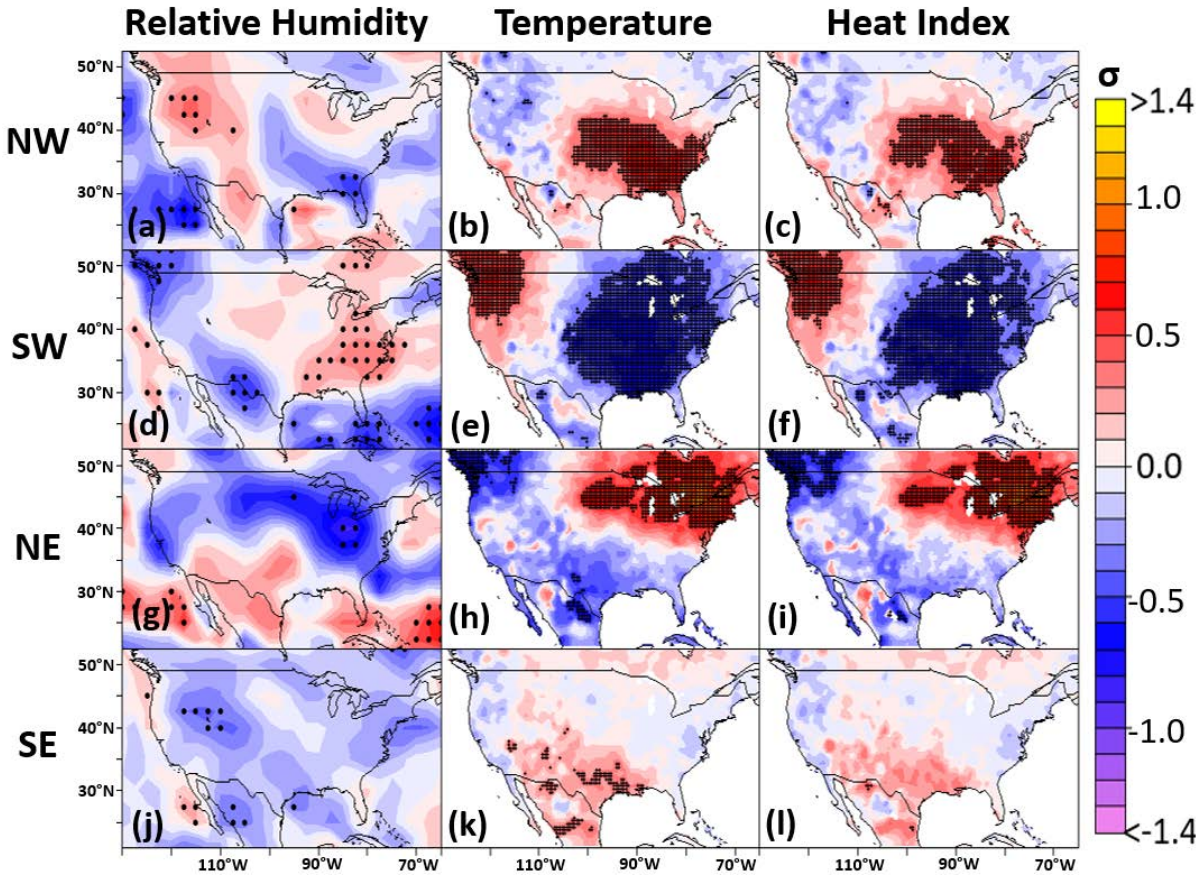

Figure 6. *Same as Figure 5, but for climate variables related to energy demand.*

A similar although weaker argument can also be made for CC2 and situations when the NASH western ridge is east of its climatological position. In particular, when the ridge sits to the NE of its mean position, precipitation decreases across most of the northern U.S. and also increases in the south, similar to the pattern under CC2 (Fig. 5i). The streamflow response, although consistent with that of precipitation, is less strong (Fig. 5j). Similarly, wind speeds increase in the northern plains and decrease over Texas (Fig. 5k), while insolation increases over the Midwest (Fig. 5l). Temperature and HI anomalies also have a similar north-south dipole to CC2, although shifted somewhat to the east. In addition, relatively humidity decreases in the north while increasing in the

south, opposing the patterns exhibited by temperature and HI (Fig. 6g-i). Importantly though, surface climate anomalies under SE ridging do not exhibit opposite patterns to NE ridging, and do not share features that are similar to the CC2 patterns, suggesting nonlinearity and asymmetric climate responses to the position of the NASH (Fig. 5m-p, Fig. 6j-l).

4.3. Impacts on Renewable Energy Supply and Demand

To relate the climate patterns identified above more directly to renewable energy infrastructure, Figures 7 and 8 show percent changes (with respect to climatology) in precipitation, wind power, insolation, and the HI at existing and potential hydropower facilities, wind turbines, solar power plants, and high-population cities, respectively, during the NW and SW ridging patterns. There is already hydropower and wind turbine infrastructure in place to leverage opposing climate patterns under these ridging typologies, suggesting there is currently the potential to partially balance renewable energy output and demand across regions of the CONUS. For instance, under the NW ridging typology, precipitation near hydropower dams in the Southeast declines by 15-20% (Fig. 7c), but this hydropower loss could potentially be balanced by 15-50% increases in wind power at turbine locations in the southern Great Plains (Fig. 7f). Wind power from the Plains could be particularly beneficial during NW ridging years because many large cities in the Southeast would also likely be experiencing an anomalously high HI (up to 65% above average, Fig. 7o). While we would expect additional solar energy production in the Southeast to offset the expected demand increase given the large increase in HI, the percent change in insolation is small (< 5%, Fig. 7k) compared

to changes in HI. The abundance of non-powering dams along the upper Mississippi River could also be retrofit with turbines to further take advantage of precipitation increases and hydropower potential in the upper Midwest (Fig. 7a) when drought strikes the Southeast under NW ridging. A similar argument could be made for wind turbines

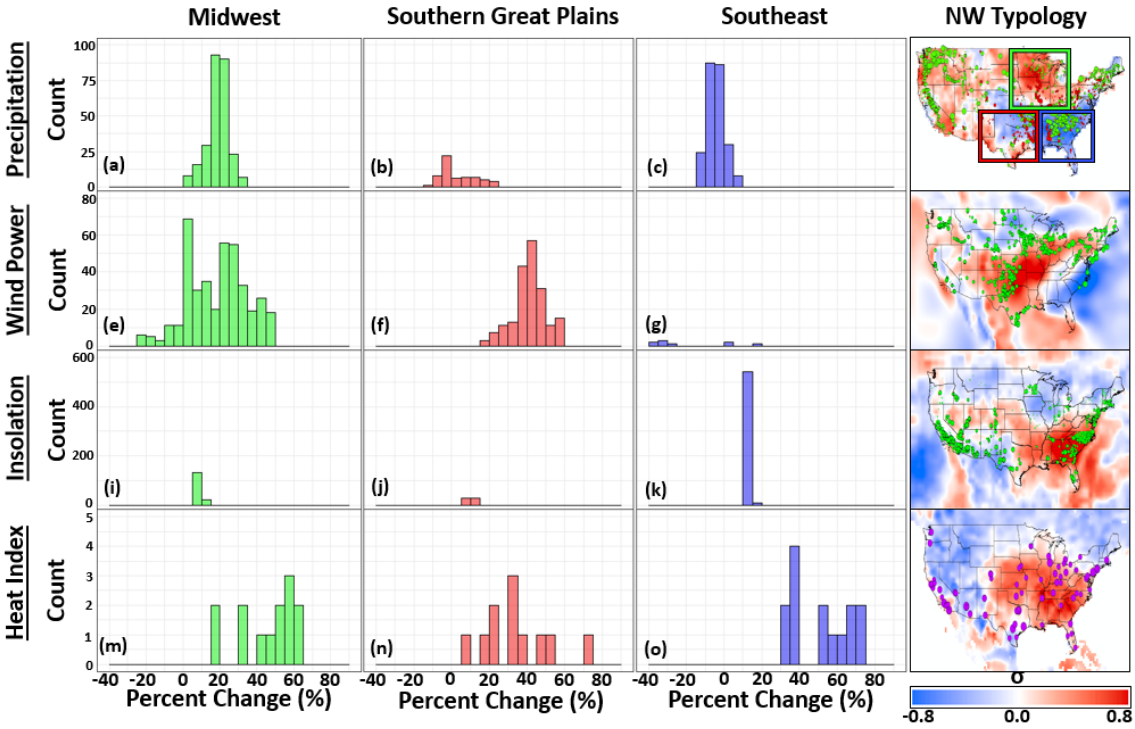

Figure 7. *The percent change (relative to the climatological mean) of a-c) precipitation, e-g) wind power (cubic of wind speed at 80 meter hub height), i-k) insolation and m-o) heat index at current and proposed infrastructure locations and major cities (d,h,l,p respectively) during the NASH NW ridging typology in the Midwest (green bars/box), southern Great Plains (red bars/box), and Southeast (blue bars/box) regions. Infrastructure mapped is d) existing hydropower infrastructure (green) and non-powering dams (red) with potential capacity scaled by size; h) wind farm sites that already exist, are proposed, or are under construction; l) existing solar power plant locations; p) major cities where populations are scaled by size. ERA Interim surface wind speeds (Dee, 2011) were used because of their finer resolution compared to the NCEP/NCAR reanalysis.*

in the Midwest (Fig. 7e). These results imply that increases in Southeastern US energy demand under NW ridging could be at least partially offset by wind energy and possibly hydropower to the north and west under a renewable energy based portfolio.

Under the SW typology, the anomalies are reverses across almost all variables, as compared to the NW typology (Fig. 8). Large decreases in wind power from the Midwest (Fig. 8e) and southern Great Plains (Fig. 8f) could be partially offset by increases in precipitation and hydropower potential from the Southeast (Fig. 8c). Exports from the Southeast may be more feasible than in an average year since demand in that region will also likely fall as HI decreases substantially (Fig. 8o) and insolation only decreases slightly (Fig. 8k). Furthermore, demands in the Midwest and the southern Great Plains would also likely be less than average due to a low HI (Fig. 8m-n), making it easier to meet these demands using power exports from the Southeast. Importantly though, the benefits offered by opposing climate patterns require sufficient long-

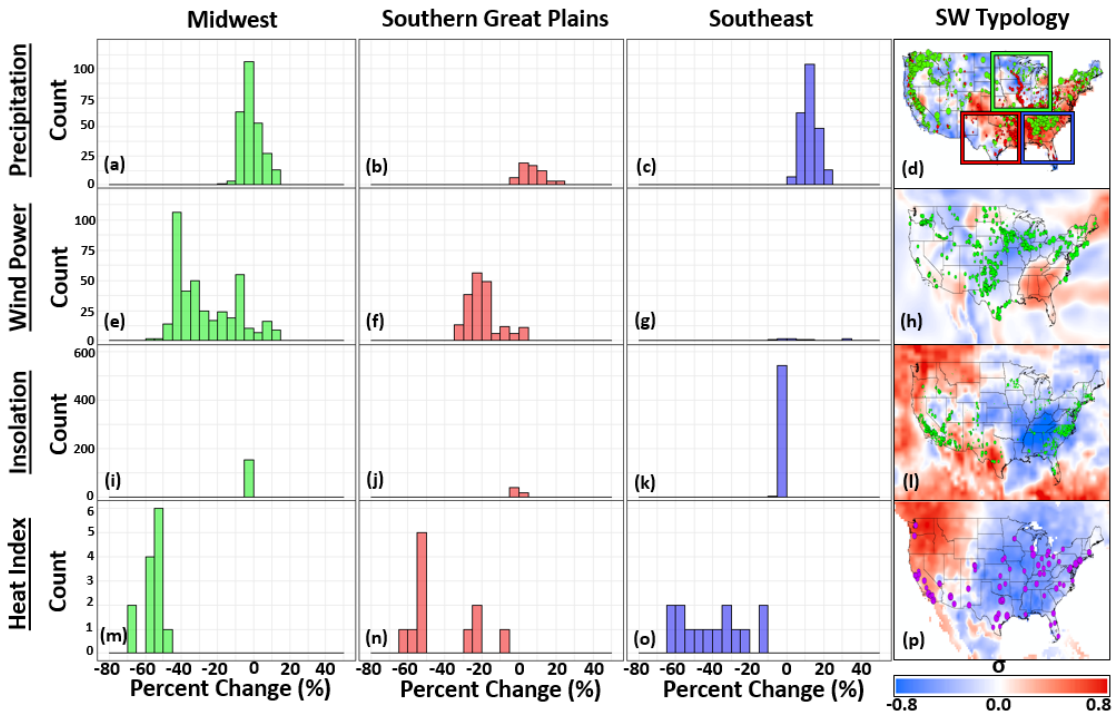

Figure 8. *Same as Figure 7, but for the NASH SW ridging typology*.

distance transmission to support an integrated power network across regions (Shaner et al. 2018), the analysis of which was beyond the scope of this study.

4.4. Large Scale Teleconnections

A Mann-Kendall test suggests no significant monotonic trend in the longitudinal position of the NASH (see Fig. 1b) over the entire 1948-2015 period (p-value = 0.1153; τ= -0.13). Therefore, to explain past variations in the NASH western ridge position, we

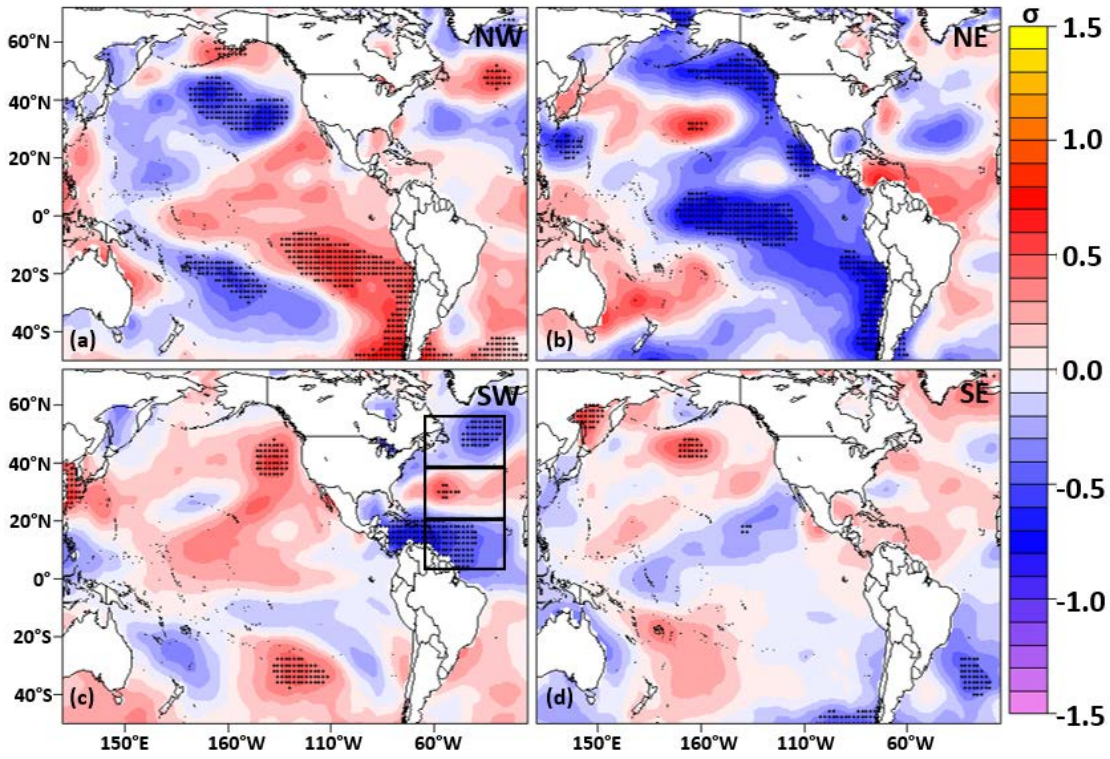

Figure 9. *Summer (JJA) sea surface temperatures composited during different phases of the NASH western ridge. The North Atlantic Tripole (NAT) is defined in the three separate boxed regions above.*

SST (JJA)	*ENSO*		*AMO*		*PDO*		*NAT*	
	Coefficient	p-value	Coefficient	p-value	Coefficient	p-value	Coefficient	p-value
NW	-0.28	0.57	-6.88	0.02**	0.42	0.24	2.14	0.22
SW	0.19	0.69	-3.56	0.25	-0.34	0.40	-3.38	0.08*
NE	0.57	0.32	-5.95	0.08*	-0.66	0.15	1.01	0.59
ATM (JJA)	*PNA*		*NAO*					
	Coefficient	p-value	Coefficient	p-value				
NW	-0.92	0.11	0.94	0.09*				
SW	-0.70	0.26	1.86	0.01**				
NE	-0.42	0.94	1.39	0.04*				

Asterisks denote significance to .05** and 0.1*

Table 2. *Multinomial regression results between JJA NASH states and JJA oceanic and atmospheric teleconnection indices.*

SST (MAM)	*ENSO*		*AMO*		*PDO*		*NAT*	
	Coefficient	p-value	Coefficient	p-value	Coefficient	p-value	Coefficient	p-value
NW	0.63	0.23	-5.62	0.05*	0.67	0.09*	0.46	0.77
SW	0.61	0.25	-3.69	0.19	0.08	0.84	-2.82	0.12
NE	0.68	0.23	-6.14	0.06*	-0.48	0.34	3.04	0.12
ATM (MAM)	*PNA*		*NAO*					
	Coefficient	p-value	Coefficient	p-value				
NW	1.24	0.03**	0.10	0.87				
SW	-0.20	0.69	0.48	0.45				
NE	1.32	0.05**	-0.48	0.52				

Asterisks denote significance to .05** and 0.1*

Table 3. *Multinomial regression results between JJA NASH states and MAM oceanic and atmospheric teleconnection indices.*

examine the relationship between different phases of the NASH and teleconnections from the Pacific and Atlantic basins. Figure 9 shows concurrent (JJA) SSTs composited during each of the four phases of the NASH western ridge, and Table 2 shows the results of two multinomial logistic regressions between these NASH states and a series of JJA oceanic and atmospheric teleconnection indices, respectively. During NW ridging, significant SST anomalies emerge in the extratropics, particularly in the Pacific, and resemble a positive PDO-like pattern (Fig. 9a). This is consistent with the signal found

in Li et al. (2012a). These SST correlations are consistent with air-sea interactions under a positive PNA, whereby atmospheric anomalies in the Aleutian Low region drive underlying SST anomalies in extratropical regions (Frankignoul 1985; Kushnir et al. 2002; Wiedermann et al. 2016). Accordingly, the multinomial regression finds a stronger relationship between NW ridging and the PNA than the PDO, although both are insignificant at the 0.1 level. NE ridging is associated with an opposite, negative PDO-like pattern, as well as stronger negative SST anomalies in the tropical Pacific (Fig. 9b), yet the coefficients on the JJA Niño 3.4, PNA, and PDO indices in the multinomial regression are insignificant. It is important to recognize that the NE ridging pattern has the fewest observations (10 years), complicating the identification of significant relationships. Interestingly, both the NW and NE ridging patterns have strong negative (positive) relationships with the AMO (NAO), with the NW pattern more strongly linked to the AMO, and the NE pattern more closely associated with the NAO. This is consistent with the SST patterns for NW ridging (Fig. 9a), as the summer AMO index shows higher SST anomalies off the west coast of Newfoundland in JJA. Overall, when the NASH western ridge is to the north of its climatological mean position, the longitudinal variability in the ridge location appears to be associated with opposing patterns in the Pacific reminiscent of the PDO, as well as SST patterns in the Atlantic, both of which are associated with larger-scale atmospheric wave patterns associated with the PNA and NAO.

When the ridge is to the south of its climatological average, Atlantic SSTs appear more strongly associated with the longitudinal position of the NASH western ridge than

Pacific SSTs. While SST anomalies during SE ridging are relatively muted (Fig. 9d), there are significant SST anomalies in the tropical North Atlantic Ocean and Caribbean Sea during SW ridging, as well as in the extratropical regions east of North America (Fig. 9c). This pattern strongly resembles the North Atlantic Tripole, which is confirmed by the statistically significant (at 90%) regression coefficient on the NAT index for SW ridging. SW ridging is also positively related to the NAO (statistically significant at 95%), which has also been shown to impose a NAT pattern in the winter and spring (Marshall et al. 2001; Seager et al. 2012). Overall, this suggests that a southwestward shift of the NASH western ridge may be linked more to an Atlantic rather than Pacific forcing, although the roles of the ocean and atmosphere in this signal are not clear.

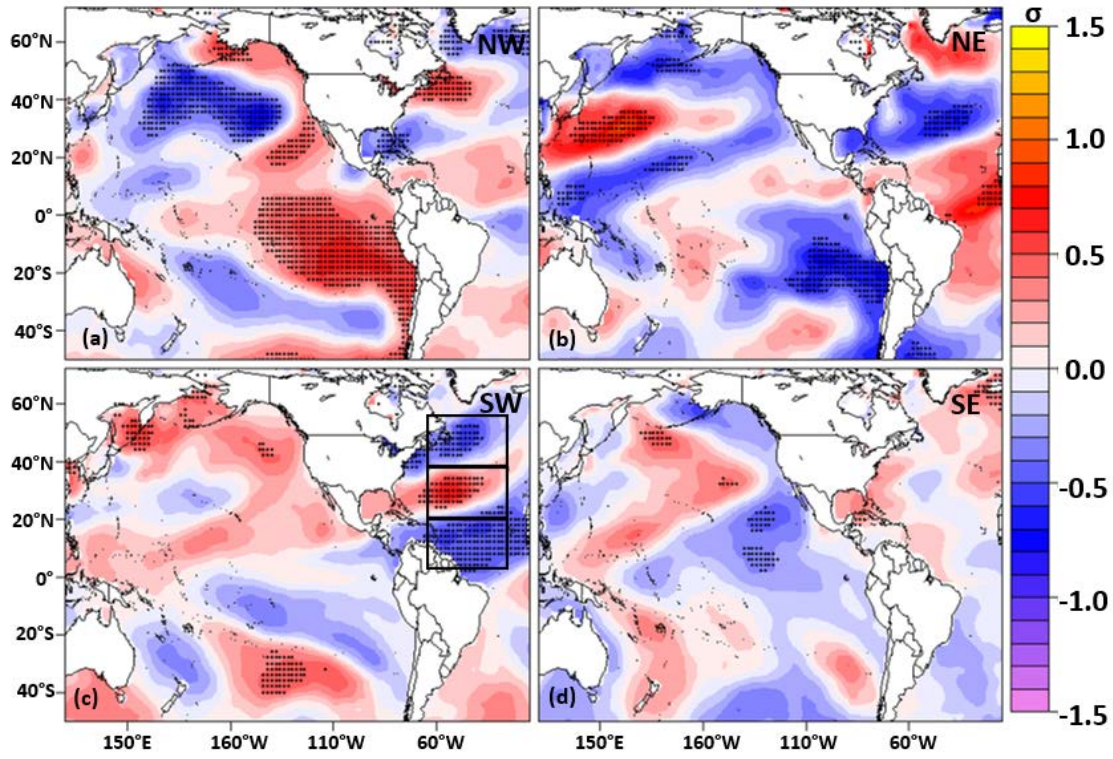

Figure 10. *As in Figure 9, but for spring (MAM) SSTs.*

To better understand whether oceanic or atmospheric forcing might provide seasonal predictability of the JJA patterns identified above, Figure 10 and Table 3 show results for the relationships between JJA phases of the NASH and lagged (MAM) climate indices. Several insights emerge from Figure 10 and Table 3. First, under NW and NE ridging, a similar PDO-like signal emerges, but the influence of the tropical Pacific becomes more pronounced, particularly for the NW typology (Fig. 10a,b). Accordingly, the coefficient on the MAM Niño 3.4 index is stronger for the NW and NE NASH states in the multinomial regression as compared to the JJA Niño 3.4 index, although the MAM coefficients still remain insignificant. In addition, the relationship between NW ridging and the MAM PDO is significant at the 0.1 level. Most notably though, there is a strong, positive, and significant relationship between the MAM PNA index and both NW and NE ridging. The NW and NE typologies also have strong relationships with MAM Atlantic SSTs, including strong regression relationships to the AMO, although with no significant relationship to the NAO. Importantly, under the NW ridging pattern all significant patterns of Atlantic SSTs are also associated with a strong, positive MAM PNA (not shown), suggesting that this Pacific wave pattern may be driving the MAM SST signals seen in Figure 10a. This may also be the case for NE ridging, although variability unique to the Atlantic may also play a larger role, given the strong relationship between the MAM NAT index and NE ridging. Overall, the results suggest that a springtime Pacific wave train, possibly initiated by ENSO and modulated by Atlantic climate, has an effect that persists into the summer to influence the NASH western ridge when it is north of its climatological average.

During SW ridging, SST anomalies in the Atlantic during MAM are similar to that in JJA, and resemble a clear NAT pattern (Fig. 10c). This is also seen in the coefficient on the MAM NAT index in the multinomial regression for the SW pattern ($p=0.12$), which is the strongest relationship seen for the SW ridging state. Importantly, both MAM atmospheric indices (PNA, NAO) are unrelated to SW ridging, even though the JJA NAO is strongly related to SW ridging. This indicates that the spring NAT may provide a feedback to the atmosphere in the following summer, and thus provide some seasonal predictability for SW ridging.

5. Discussion

Results show that NW and NE ridging patterns are associated with both Pacific and Atlantic climate variability in the summer, and are strongly related to a PNA-based atmospheric wave pattern and the AMO in the preceding spring. This suggests that springtime, synoptic-scale climate variability in the Pacific and SST variability in the Atlantic could be used to predict these NASH states and their associated surface climate in the following summer. For SW ridging, the strongest relationship emerged for the summer NAO, while a springtime NAT pattern provided the most seasonal predictability. The NAT has been previously shown to represent the SST response to a winter NAO (Marshall et al. 2001) and mid-tropospheric height anomalies off the eastern coast of Newfoundland in the spring (Seager et al. 2012), but also has been linked with feedbacks on atmospheric circulation in the spring (Peng et al. 2002) and summer (Gastineau and Frankignoul 2015). Past work has also shown that NAT anomalies in the spring have a link to streamflow anomalies over the Northeast U.S.

during the following summer (Steinschneider and Brown 2011; Steinschneider and Brown 2012; Ahn et al. 2017). Given the positive precipitation and streamflow anomalies seen during SW NASH ridging in the Northeast US (see Fig. 5e,f), this suggests that the influence of the MAM NAT on the orientation of the NASH may at least partially explain the forecasting signals identified in those previous studies. All of the forecasting signals mentioned above could be used to inform season-ahead planning for energy systems, such as tailoring the price of demand-response contracts (Cardell and Anderson 2015) based on the risk of high peak energy loads or renewable energy supply reductions in the coming summer season. One limitation of our approach and the identified forecasting signals is the limited number of available years for each NASH typology, which ranged from 10 (NE) to 18 (SW) years. Future work should utilize numerical experiments from coupled climate models to confirm the relationship between NASH ridging and different modes of Atlantic and Pacific climate variability.

The results are also consistent with past work that has linked variability in the NASH specifically to variations in tropical Atlantic SSTs. Modeling experiments suggest that colder (warmer) Caribbean and tropical Atlantic waters incite a Gill-type sea level pressure response (Gill 1980) over the Gulf of Mexico that strengthens (weakens) the NASH and displaces its core to the southwest (northeast) (Wang and Lee 2007; Wang et al. 2008; Weaver et al. 2009; Kushnir et al. 2010). Thus, the intensity of the NASH, as forced in part by an underlying SST anomaly, may impact whether a SW ridging event emerges (Li et al. 2012a). Importantly, decadal-scale persistence in tropical Atlantic SSTs can excite this Gill-type response persistently from year to year (Weaver

et al. 2009; Schubert et al. 2009; Kushnir et al. 2010; Seager and Hoerling 2014), suggesting that the joint distribution of surface climate linked to westward and eastward positions of the NASH western ridge could also exhibit decadal scale variability. This behavior not only has implications for the stability of summertime renewable energy generation and demand across the eastern U.S., but also could complicate the detection of longer-term changes in the NASH position forced by anthropogenic climate change (Li et al. 2012b; Thibeault and Seth 2014; Thibeault and Seth 2015; Ryu and Hayhoe 2017). For instance, Li et al. (2011, 2012a) observed westward movement of the western ridge of the NASH for the period from 1978-2007 as compared to the 1948-1977 period. In apparent disagreement, Diem (2011) found the western ridge of the NASH trending eastward from the late 1970's to 2010. Through our extension of the western ridge location up until 2015 (Fig. 1b), we observe that in 6 of the last 8 years following 2007 the western ridge was located east of its mean climatological position, and there was no significant long-term trend in the longitudinal position of the NASH. Though a definitive pattern cannot be inferred from this short extension, the addition of this most recent data suggests that any trends in the east-west displacement of the NASH western ridge, if present, are masked by a substantial amount of natural, decadal-scale variability. If long-term trends could be confidently established, the surface climate relationships linked to variability in the NASH could help in the development of infrastructure and policy to mitigate the effects of long-term climate change by improving the inter-annual reliability of existing and potential future renewable energy infrastructure in the U.S. However, the climate response reported in this study is not necessarily linearly associated with continued westward movement of the NASH

western ridge, and so further research is needed to quantify changes in surface climate under potential orientations of the NASH not previously seen in the historic record.

6. Conclusion

This study is the first to demonstrate substantial, pan-continental coherence in the largest modes of joint variability between a suite of summertime hydrometeorological variables across the CONUS that are directly relevant to renewable energy supply and demand, and their link to the orientation of the western ridge of the North Atlantic subtropical high. Different typologies of NASH ridging were found to be associated with changes in temperature and insolation, atmospheric flow, and moisture from the Gulf of Mexico over the Eastern US, providing opportunities to balance renewable energy production and demand across different regions of the country. Certain patterns in NASH ridging are also related to lagged, large-scale patterns of Pacific and Atlantic atmospheric and oceanic variability, raising the potential for seasonal forecasts that could inform renewable energy system management. Existing renewable energy infrastructure and sites of high energy demand are found to already be in locations that could leverage coherent climate patterns for certain NASH typologies. However, sufficient long-distance transmission would be required to support such a strategy. The cost-benefit analysis of developing that transmission system (given existing long-distance transmission lines) versus the reliability provided through balancing renewables is currently unknown. We leave this assessment for future work.

ACKNOWLEDGMENTS

The CPC US Unified Precipitation, GHCN+CAMS temperature and NCEP Reanalysis Derived data provided by the NOAA/OAR/ESRL PSD, Boulder, Colorado, USA, from their Web site at http://www.esrl.noaa.gov/psd/. The Surface Radiation Budget insolation data was obtained from the NASA Langley Research Center Atmospheric Science Data Center at https://eosweb.larc.nasa.gov/project/srb/srb_table.

REFERENCES

Abhishek, A., Lee, J. Y., Keener, T. C., & Yang, Y. J. (2010). Long-Term Wind Speed Variations for Three Midwestern US Cities *Journal of the Air & Waste Management Association*, **60** 1057-1064. https://doi.org/10.1002/qj.828

Ahn, K.-H., R. Palmer, and S. Steinschneider (2017), A hierarchical Bayesian model for regionalized seasonal forecasts: Application to low flows in the northeastern United States, *Water Resour. Res*., **53**, 503–521, doi:10.1002/2016WR019605.
Barlow, M., Nigam, S. & Berbery, E. H., (2001). ENSO, Pacific Decadal Variability, and U.S. Summertime Precipitation, Drought, and Stream Flow. *Journal of Climate*, **14** 2105-2128. https://doi.org/10.1175/1520-0442(2001)014<2105:EPDVAU>2.0.CO;2

Barry, R.G., Kiladis, G., & Bradley, R.S. (1981). Synoptic climatology of the Western United States in relation to climatic fluctuations during the twentieth century. *Journal of Climatology*, **1**, 97-113. https://doi.org/10.1002/joc.3370010202

Barnston, A. G., and R. E. Livezey (1987), Classification, seasonality and persistence of low-frequency atmospheric circulation patterns. *Monthly Weather Review*, **115**, 1083-1126.

Bartos, M., Chester, M., Johnson, N., Gorman, B., Eisenberg, D., Linkov, I., et al. (2016). Impacts of rising air temperatures on electric transmission ampacity and peak electricity load in the United States. *Environmental Research Letters*, **11,** 114008. https://doi.org/10.1088/1748-9326/11/11/114008

Bélanger, C., & Gagnon, L. (2002). Adding wind energy to hydropower. *Energy Policy*, **30**, 1279-1284. https://doi.org/10.1016/S0301-4215(02)00089-7

Bett, P. E., & Thornton, H. E. (2016). The climatological relationships between wind and solar energy supply in Britain. *Renewable Energy*, **87**, 96–110. https://doi.org/10.1016/j.renene.2015.10.006

Bichet, A., Wild, M., Folini, D., Schär, C. (2012). Causes for decadal variations of wind speed over land: Sensitivity studies with a global climate model. *Geophysical Research Letters*, **39**, 4–9. https://doi.org/10.1029/2012GL051685

Bloomfield, H., Brayshaw, D. J., Shaffrey, L. C., Coker, P. J., & Thornton, H. E. (2018). The changing sensitivity of power systems to meteorlogical drivers: a case study of Great Britain. *Environmental Research Letters*, **13**, 054028. https://doi.org/10.1088/1748-9326/aabff9

Brazel, A.J., & Nickling, W.G. (1986). The relationship of weather types to dust storm generation in Arizona (1965-1980). *Journal of Climatology*, **6**, 255-275. https://doi.org/10.1002/joc.3370060303

Cardell, J. B., & Anderson, C. L. (2015). A Flexible Dispatch Margin for Wind Integration. *IEEE Transactions on Power Systems*, **30**, 1501–1510. https://doi.org/10.1109/TPWRS.2014.2337662

Castronuovo, E. D., & Lopes, J. A. P. (2004). On the optimization of the daily operation of a wind-hydro power plant. *IEEE Transactions on Power Systems*, **19**, 1599–1606. https://doi.org/10.1109/TPWRS.2004.831707

Chang, M. K., Eichman, J. D., Mueller, F., & Samuelsen, S. (2013). Buffering intermittent renewable power with hydroelectric generation: A case study in California. *Applied Energy*, **112**. https://doi.org/10.1016/j.apenergy.2013.04.092

Chen, M., Shi, W., Xie, P., Silva V. B. S., Kousky, R., Higgins, W., et al. (2008), Assessing objective techniques for gauge-based analyses of global daily precipitation, *Jouranl of Geophysical Research*, **113**. https://doi.org/10.1029/2007JD009132

Cherry, J., Cullen, H., Visbeck, M., Small, A., & Uvo, C. (2005). Impacts of the North Atlantic oscillation on scandinavian hydropower production and energy markets. *Water Resources Management*, **19**, 673–691. https://doi.org/10.1007/s11269-005-3279-z

Crimmins, M. (2006). Synoptic climatology of extreme fire-weather conditions across the southwest United States. *International Journal of Climatology*, **26**, 1001-1016. https://doi.org/10.1002/joc.1300

Cropper, T., Hanna, E., Valente, M. A., Jonsson, T. (2015). A daily Azores-Iceland North Atlantic Oscillation index back to 1850. *Geoscience Data Journal*, **2**, 12-24. http://doi.org/10.1002/gdj3.23

Cross, B. D., Kohfeld, K. E., Bailey, J., & Cooper, A. B. (2015). The impacts of wind speed trends and 30-year variability in relation to hydroelectric reservoir inflows on wind power in the Pacific Northwest. *PLoS ONE*, **10**, 1–22. https://doi.org/10.1371/journal.pone.0135730

Davis, R.E., & Walker, D.R. (1991). An Upper-Air Synoptic Climatology of the Western United States. *Journal of Climate*, **5**, 1449-1467. https://doi.org/10.1175/1520-0442(1992)005<1449:AUASCO>2.0.CO;2

Davis, R.E., Hayden, B.P., Gay, D.A., Phillips, W.L., & Jones, G.V. (1997), The North Atlantic subtropical anticyclone, *Journal of Climate*, **10**, 728-744. https://doi.org/10.1175/1520-0442(1997)010<0728:TNASA>2.0.CO;2

DeCarolis, J. F., & Keith, D. W. (2006). The economics of large-scale wind power in a carbon constrained world. *Energy Policy*, **34**, 395–410. https://doi.org/10.1016/j.enpol.2004.06.007

Dee, D. P., Uppala, S. M., Simmons, A. J., Berrisford, P., Poli, P., Kobayashi, S., et al. (2011), The ERA-Interim reanalysis: configuration and performance of the data assimilation system. *Quarterly Journal of the Royal Meteorological Society*, **137**, 553–597. https://doi.org/10.1002/qj.828

Diem, J. E. (2006). Synoptic-scale controls of summer precipitation in the southeastern United States. *Journal of Climate*, **19**, 613–621. https://doi.org/10.1175/JCLI3645.1

Diem, J. E. (2011) Influences of the Bermuda High and atmospheric moistening on changes in summer rainfall in the Atlanta Georgia region, USA, *International Journal of Climatology*, **33**, 160-172. https://doi.org/10.1002/joc.3421

DNV-GL (2016), Whither the winds in 2015? Analysis of the anomalously low winds across the U.S., Report No. 108917-R-01-A.

Draxl, C., Clifon, A., Hodge, B.M., & McCaa, J. (2015). "The Wind Integration National Dataset (WIND) Toolkit." *Applied Energy*,**151**, 355366. https://doi.org/10.1016/j.apenergy.2015.03.121

Dunn, B., Kamath, H., & Tarascon, J.-M. (2011). Electrical Energy Storage for the Grid: A Battery of Choices. *Science*, **334**, 928–935. https://doi.org/10.1126/science.1212741

Ely, C. R., Brayshaw, D. J., Methven, J., Cox, J., & Pearce, O. (2013). Implications of the North Atlantic Oscillation for a UK–Norway renewable power system. *Energy Policy*, **62**, 1420-1427. https://doi.org/10.1016/j.enpol.2013.06.037

Energy Information Administration (2015). California's continued drought, reduced snowpack mean lower hydropower output. Today in Energy. Available at https://www.eia.gov/todayinenergy/detail.php?id=20732

Energy Information Administration (2017). Independent Statistics & Analysis. (Annual Summary 2005-2017)

Energy Information Administration (2018). U.S. Energy Mapping System, Retrieved from https://www.eia.gov/state/maps.php?v=Electricity

Enfield, D. B., Mestas-Nuñez, A. M., Trimble, P. J. (2001) The Atlantic multidecadal oscillation and its relation to rainfall and river flows in the continental U.S.

Geophysical Research Letters, **28**, 2077-2080.
http://dx.doi.org/10.1029/2000GL012745.

Engeland, K., Borga, M., Creutin, J., François, B., Ramos, M., Vidal, J. (2017). Space-time variability of climate variables and intermittent renewable electricity production – A review. *Renewable and Sustainable Energy Reviews*, **79**, 600-617. http://dx.doi.org/10.1016/j.rser.2017.05.046

Ewen, T., Brönnimann, S., & Annis, J. (2008). An Extended Pacific-North American Index from Upper-Air Historical Data Back to 1922. *Journal of Climate*, **21**, 1295-1308. https://doi.org/10.1175/2007JCLI1951.1

Falcone, J. A., Carlisle, D. M., Wolock, D. M., & Meador, M. R. (2010). GAGES: A stream gage database for evaluating natural and altered flow conditions in the conterminous United States. *Ecology*, **91**(2), 621-621.

Fan, Y., & van den Dool, H. (2008). A global monthly land surface air temperature analysis for 1948-present. *Journal of Geophysical Research Atmospheres*, **113**, 1–18. https://doi.org/10.1029/2007JD008470

Fernandez, A.R., Blumsack, S.A., & Reed, P.M. (2012), Evaluating wind-following and ecosystem services for hydroelectric dams in PJM, *Proceedings of the Annual Hawaii International Conference on System Sciences*, **41**, 1897-1906. https://doi.org/10.1109/HICSS.2012.256

Fernandez, A. R., Blumsack, S. A., & Reed, P. M. (2013). Operational constraints and hydrologic variability limit hydropower in supporting wind integration. *Environmental Research Letters*, **8**, 24037. https://doi.org/10.1088/1748-9326/8/2/024037

Fertig, E., Apt, J., & Jaramillo, P., Katzenstein, W. (2012). The effect of long-distance interconnection on wind power variability. *Environmental Research Letters*, **7**, 34017. https://doi.org/10.1088/1748-9326/7/3/034017

Gastineau, G., and C. Frankignoul (2015), Influence of the North Atlantic SST variability on the atmospheric circulation during the twentieth century, *Journal of Climate*, **28**, 1396–1416.

Gill, A. E. (1980). Some simple solutions for heat-induced tropical circulation, *Quarterly Journal of the Royal Meteorological Society*, **106**, 447–462. https://doi.org/10.1002/qj.49710644905

Gimeno, L., A. Drumond, R. Nieto, R. M. Trigo, and A. Sthol (2010), On the origin of continental precipitation. *Geophysical Research Letters*, **37**, L13804, doi:10.1029/2010GL043712.

González, I., Déjean S, Martin P.G.P., Baccini, A. (2008) CCA: An R package to extend canonical correlation analysis. *Journal of Statistical Software*, **23**, 1–14.

Goodrich, G. B. (2007). Influence of the Pacific Decadal Oscillation on Winter Precipitation and Drought during Years of Neutral ENSO in the Western United States. *Weather and Forecasting*, **22**, 116-124. https://doi.org/10.1175/WAF983.1

Greenblatt, J. B., Succar, S., Denkenberger, D. C., Williams, R. H., & Socolow, R. H. (2007). Baseload wind energy: modeling the competition between gas turbines and compressed air energy storage for supplemental generation. *Energy Policy*, **35**, 1474-1492. https://doi.org/10.1016/j.enpol.2006.03.023

Hadjerioua, B., Wei, Y., & Kao, S.-C. (2012). An assessment of energy potential at non-powered dams in the United States. Report by Oak Ridge National Laboratory for U.S. Department of Energy. https://doi.org/10.2172/1039957

Hamlington, B. D., P. E. Hamlington, S. G. Collins, S. R. Alexander, & K.-Y. Kim (2015). Effects of climate oscillations on wind resource variability in the United States, *Geophysical Research Letters*, **42**, 145–152. https://doi.org/10.1002/2014GL062370

Hasanean, H.M. (2004). Variability of the North Atlantic subtropical high and associations with tropical sea-surface temperature, *International Journal of Climatology*, **24**, 945-957. https://doi.org/10.1002/joc.1042

Haupt, S. E., Copeland, J., Cheng, W. Y. Y., Zhang, Y., Ammann, C., & Sullivan, P. (2016). A method to assess the wind and solar resource and to quantify interannual variability over the United States under current and projected future climate. *Journal of Applied Meteorology and Climatology*, **55**, 345–363. https://doi.org/10.1175/JAMC-D-15-0011.1

Hirth, L. (2016). The benefits of flexibility: The value of wind energy with hydropower. *Applied Energy*, **181**, 210–223. https://doi.org/10.1016/j.apenergy.2016.07.039

Hittinger, E., Whitacre, J. F., & Apt, J. (2010). Compensating for wind variability using co-located natural gas generation and energy storage. *Energy Systems*, **1**, 417–439. https://doi.org/10.1007/s12667-010-0017-2

Ho, M., U. Lall, & E. R. Cook (2016), Can a paleodrought record be used to reconstruct streamflow?: A case study for the Missouri River Basin. *Water Resources Research*, **52**, 5195-5212. https://doi.org/10.1002/2015WR018444

Huang, B., Banzon, V.F., Freeman, E., Lawrimore, J., Liu, W., Peterson, T.C., Smith, T.M., Thorne, P.W., Woodruff, S.D., and Zhang, H.M. (2014). Extended

Reconstructed Sea Surface Temperature version 4 (ERSST.v4): Part I. Upgrades and intercomparisons. *Journal of Climate*, **28**, 911-930, https://doi.org/10.1175/JCLI-D-14-00006.1

Huang, B., P. Thorne, T. Smith, W. Liu, J. Lawrimore, V. Banzon, H. Zhang, T. Peterson, and M. Menne, 2015: Further Exploring and Quantifying Uncertainties for Extended Reconstructed Sea Surface Temperature (ERSST) Version 4 (v4). *Journal of Climate*, in press, doi:10.1175/JCLI-D-15-0430.1

Jerez, S., & Trigo, R. M. (2013). Time-scale and extent at which large-scale circulation modes determine the wind and solar potential in the Iberian Peninsula. *Environmental Research Letters*, **8**, 1-11. https://doi.org/10.1088/1748-9326/8/4/044035

Jerez, S., Trigo, R. M., Vicente-Serrano, S. M., Pozo-Vázquez, D., Lorente-Plazas, R., Lorenzo-Lacruz, J., Santos-Alamillos, F. & Montávez, J. P. (2013). The impact of the North Atlantic Oscillation on renewable energy resources in southwestern Europe. *Journal of Applied Meteorology and Climatology*, **52**, 2204-2225. https://doi.org/10.1175/JAMC-D-12-0257.1

Kalnay, E., et al. (1996). The NCEP/NCAR 40-year reanalysis project. *Bulletin of the American Meteorological Society*, **77**,437-471. https://doi.org/10.1175/1520-0477(1996)077<0437:TNYRP>2.0.CO;2

Kaplan, A., Cane, M., Kushnir, Y., Clement, A., Blumenthal, M., & Rajagopalan, B. (1998), Analyses of global sea surface temperature 1856-1991, *Journal of Geophysical Research*, **103**, 18,567-18,589. https://doi.org/10.1029/97JC01736
Kirchner-Bossi, N., García-Herrera, R., Prieto, L., & Trigo, R. M. (2015). A long-term perspective of wind power output variability. *International Journal of Climatology*, **35**, 2635–2646. https://doi.org/10.1002/joc.4161

Kosnik, L. (2010). The potential for small scale hydropower development in the US. *Energy Policy*, **38**, 5512–5519. https://doi.org/10.1016/j.enpol.2010.04.049

Kushnir, Y., Robinson, W.A., Blade, I., Hall, N.M.J., Peng, S., & Sutton, R. (2002). Atmospheric GCM response to extratropical SST anomalies: synthesis and evaluation, *Journal of Climate*, **15**, 2233-2256.

Kushnir, Y., R. Seager, M. Ting, N. Naik, & J. Nakamura (2010), Mechanisms of tropical Atlantic SST influence on North American precipitation variability, *Journal of Climate*, **23**, 5610-5628. https://doi.org/10.1175/2010JCLI3172.1

Leurgans, E., Moyeed, A., Silverman, B., (1993), Canonical correlation analysis when the data are curves, *Journal of the Royal Statistical Society*, **55**, 725-740.

Li, W., Li, L., Fu, R., Deng, Y., & Wang, H. (2011). Changes to the North Atlantic Subtropical High and Its Impact on Summer Droughts / Floods in the Southeastern US Scientific Questions. *Journal of Climate*, **24**, 431004. https://doi.org/10.1175/JCLI-D-11-00674.1

Li, L., Li, W., & Kushnir, Y. (2012a). Variation of the North Atlantic subtropical high western ridge and its implication to Southeastern US summer precipitation. *Climate Dynamics*, **39**, 1401–1412. https://doi.org/10.1007/s00382-011-1214-y

Li, W., Li, L., Ting, M., & Liu, Y. (2012b). Intensification of Northern Hemisphere subtropical highs in a warming climate. *Nature Geoscience*, **5**,830–834. https://doi.org/10.1038/ngeo1590

Li, L., Schmidt, R. W., & Ummenhofer, C. C. (2017). The role of the subtropical North Atlantic water cycle in recent US extreme precipitation events. *Climate Dynamics*, 1-15. https://doi.org/10.1007/s00382-017-3685-y

Li, X., Zhong, S., Bian, X., & Heilman, W. E. (2010). Climate and climate variability of the wind power resources in the Great Lakes region of the United States. *Journal of Geophysical Research Atmospheres*, **115**, 1–15. https://doi.org/10.1029/2009JD013415

Liu, W., B. Huang, P.W. Thorne, V.F. Banzon, H.-M. Zhang, E. Freeman, J. Lawrimore, T.C. Peterson, T.M. Smith, and S.D. Woodruff, 2014: Extended Reconstructed Sea Surface Temperature version 4 (ERSST.v4): Part II. Parametric and structural uncertainty estimations. *Journal of Climate*, 931-951, doi:10.1175/JCLI-D-14-00007.1

Livneh, B., Rosenberg, E. A., Lin, C., Nijssen, B., Mishra, V., Andreadis, K. Maurer. E & Lettenmaier, D. P. (2013). A long-term hydrologically based dataset of land surface fluxes and states for the conterminous United States: Update and extensions. *Journal of Climate*, **26**, 9384–9392. https://doi.org/10.1175/JCLI-D-12-00508.1

Mann, H.B. (1945). Non-parametric tests against trend, *Econometrica*, **13**,163-171, doi: 10.2307/1907187

Mantua, N. J., Hare, S. R., Zhang, Y., Wallace, J. M., & Francis, R. C. (1997). A Pacific Interdecadal Climate Oscillation with Impacts on Salmon Production. *American Meteorological Society*, **78**, 1069-1079. https://doi.org/10.1175/1520-0477(1997)078<1069:apicow>2.0.co;2

Marshall, J., Kushnir, Y., Battisti, D., Chang, P., Czaja, A., Dickson, R., Hurrell, J.,McCartney, M., Saravanan, R., Visbeck, M., (2001), North Atlantic climate

variability: phenomena, impacts and mechanisms. *International Journal of Climatology*, **21** (15), 1863–1898.

Miles, E. L., Snover, A. K., Hamlet, A. F., Callahan, B., & Fluharty, D. (2000). Pacific Northwest Regional Assessment: The Impacts of Climate Variability and Climate Change on the Water Resources of the Columbia River Basin. *Journal of the American Water Resources Association*, **36**, 399–420. https://doi.org/10.1111/j.1752-1688.2000.tb04277.x

Mohammadi, K., & Goudarzi, N. (2018a), Study of inter-correlations of solar radiation, wind speed, and precipitation under the influence of El Niño Southern Oscillation (ENSO) in California, *Renewable Energy*, **120**, 190-200. https://doi.org/10.1016/j.renene.2017.12.069

Mohammadi, K., & Goudarzi, N. (2018b), Association of direct normal irradiance with El Niño Southern Oscillation and its consequences on concentrated solar power production in the US Southwest, *Applied Energy*, **212**, 1126-1137. https://doi.org/10.1016/j.apenergy.2017.12.102

Monforti, H., Huld, T., Bódis, K., Vitalic, L., D'Isidoro, M., & Lacal-Arántegui, R., (2014). Assessing complementarity of wind and solar resources for energy production in Italy. A Monte Carlo approach, *Renewable Energy*, **63**, 576-586. https://doi.org/10.1016/j.renene.2013.10.028

Nobre, C.A., Marengo, J.A., Seluchi, M.E., Cuartas, L.A. & Alves, L.M. (2016) Some Characteristics and Impacts of the Drought and Water Crisis in Southeastern Brazil during 2014 and 2015. *Journal of Water Resource and Protection*, **8**, 252-262. https://doi.org/10.4236/jwarp.2016.82022

Peng, S. W. A. Robinson, and S. Li (2002), North Atlantic SST forcing of the NAO and relationships with intrinsic hemispheric variability. *Geophysical Research Letters*, **29**, 1276, doi:10.1029.2001GL014043.
Piechota, T. C. and Dracup, J. A. (1996). Drought and Regional Hydrologic Variation in the United States: Associations with the El Niño-Southern Oscillation. *Water Resources Research*, **32**, 1359-1373.

Poli, P. *et al* (2016). ERA-20C: An Atmospheric Reanalysis of the Twentieth Century, *Journal of Climate*, **29**, 4083-4097. https://doi.org/10.1175/JCLI-D-15-0556.1

Ronalds, B.F., Wonhas, A., Troccoli, A. (2014). A New Era for Energy and Meteorology. Troccoli, L. Dubus, S.E. Haupt (Ed.). *Weather Matters for Energy* (pp.3-14). New York, NY: Springer, New York.

Ropelewski, C.F., and Halpert, M.S. (1986), North American precipitation and temperature patterns associated with the El Niño/Southern Oscillation (ENSO), *Monthly Weather Review*, **114**, 2352-2362.

Ryu, J., and Hayhoe, K. (2017). Observed and CMIP5 modeled influence of large-scale circulation on summer precipitation and drought in the South-Central United States. *Climate Dynamics*, **49**, 4293-4310. https://doi.org/10.1007/s00382-017-3805-8

Sandt, C. J., Doyle, M. W. (2013). The hydrologic and economic feasibility of micro hydropower upfitting and integration of existing low-head dams in the United States. *Energy Policy*, **63**, 261–271. https://doi.org/10.1016/j.enpol.2013.08.087

Santos-Alamillos, F. J., Pozo-Vazquez, D., Ruiz-Arias, J. A., Lara-Fanego, V., & Tovar-Pescador, J. (2012). Analysis of spatiotemporal balancing between wind and solar energy resources in the southern Iberian Peninsula. *Journal of Applied Meteorology and Climatology*, **51**, 2005–2024. https://doi.org/10.1175/JAMC-D-11-0189.1

Schubert et al. (2009), A U.S. CLIVAR project to assess and compare the responses of global climate models to drought-related SST forcing patterns: overview and results, *Journal of Climate*, **22**, 5251-5272. https://doi.org/10.1175/2009JCLI3060.1

Seager, R., & M. Hoerling (2014), Atmosphere and ocean origins of North American droughts, *Journal of Climate*, **27**, 4581-4606. https://doi.org/10.1175/JCLI-D-13-00329.1

Seager, R., Hoerling, M., Schubert, S., Wang, H., Lyon, B., Kumar, A. et al. (2015). Causes of the 2011-14 California drought. *Journal of Climate*, **28**, 6997–7024. https://doi.org/10.1175/JCLI-D-14-00860.1

Seager, R., N. Pederson, Y. Kushnir, J. Nakamura, and S. Jurburg (2012), The 1960s drought and the subsequent shift to a wetter climate in the Catskill mountains region of the New York city Watershed*, *Journal of Climate*, **25**, 6721–6742.

Shaner, M. R., Davis, S.J., Lewis, N.S., & Caldeira, K. (2018). Geophysical constraints on the reliability of solar and wind power in the United States. *Energy & Environmental Science*, 914-925. https://doi.org/10.1039/C7EE03029K

Sims, R. (2014). Renewable Energy and Climate Change Mitigation: An Overview of the IPCC Special Report. In A. Troccoli, L. Dubus, S.E. Haupt (Ed.). *Weather Matters for Energy* (pp.91-110). New York, NY: Springer, New York.

Smith, J., & Baeck, M., (2017) "Strange Floods: Downscaling Simulations of the Storms that Produce Them", *American Meteorological Society*, Washington State Convention Center, Seattle, WA

SRB Science Team (2010), SRB Data, Hampton, VA, USA: NASA Atmospheric Science Data Center (ASDC), Accessed 2017-3-7 at doi: 10.5067/SRB/REL3.0_SW_MONTHLY_UTC_ NC_L3

Steinschneider, S., and C. Brown (2011), Influences of North Atlantic climate variability on low-flows in the Connecticut River Basin, *Journal of Hydrology*, **409**(1), 212–224.

Steinschneider, S., and C. Brown (2012), Forecast-informed low-flow frequency analysis in a Bayesian framework for the northeastern United States, *Water Resources Research*, **48**, W10545, doi:10.1029/2012WR011860.

Swain, D. L., D. E. Horton, D. Singh, and N. S. Diffenbaugh (2016), Trends in atmospheric patterns conducive to seasonal precipitation and temperature extremes in California, *Scientific Advances*, **2**, e1501344, doi:10.1126/sciadv.1501344.

Thibeault, J. M., & Seth, A. (2014). A framework for evaluating model credibility for warm-season precipitation in Northeastern North America: A case study of CMIP5 simulations and projections. *Journal of Climate*, **27**, 493–510. https://doi.org/10.1175/JCLI-D-12-00846.1

Thibeault, J. M., & Seth, A. (2015). Toward the credibility of Northeast United States summer precipitation projections in CMIP5 and NARCCAP simulations. *Journal of Geophysical Research: Atmospheres*, **120**, 10050–10073. https://doi.org/10.1002/2015JD023177

Thornton, H. E., Scaife, A. A., Hoskins, B. J., & Brayshaw, D. J. (2017). The relationship between wind power, electricity demand and winter weather patterns in Great Britain. *Environmental Research Letters*, **12**, 064017. https://doi.org/10.1088/1748-9326/aa69c6

Trenberth, K. E., Branstator, G. W. & Arkin, P. A. (1988). Origins of the 1988 North American Drought. *Science*, **242**, 1640-1645.

Trenberth, K. (1997). The definition of El Nino. *Bulletin of the American Meteorological Society*. 2771-2777. https://doi.org/10.1175/1520-0477(1997)078<2771:TDOENO>2.0.CO;2

U.S. Census Bureau (2015). *USA Major Cities*, Retrieved from http://www.arcgis.com/home/item.html?id=4e02a13f5ec6412bb56bd8d3dadd59dd

US Department of Energy. (2016). Hydropower Vision: Chapter 3: Assessment of National Hydropower Potential. Retrieved from http://energy.gov/eere/water/articles/hydropower-vision-new-chapter-america-s-1st-renewable-electricity-source

Vazquez, S., Lukic, S. M., Galvan, E., Franquelo, L. G., & Carrasco, J. M. (2010). Energy Storage Systems for Transport and Grid Applications. *IEEE Transactions on Industrial Electronics*, **57**, 3881–3895. https://doi.org/10.1109/TIE.2010.2076414

Vinod, H., (1976), Canonical ridge and econometrics of joint production, *Journal of Econometrics*, **6**, 129-137. https://doi.org/10.1016/0304-4076(76)90010-5

Wang, C., & Lee, S. (2007), Atlantic warm pool, Caribbean low- level jet, and their potential impact on Atlantic hurricanes, *Geophysical Research Letters*, **34**, L02703, https://doi.org/10.1029/2006GL028579.

Wang, C., & Lee, S., & Enfield, D., (2008), Atlantic warm pool acting as a link between Atlantic multidecadal oscillation and Atlantic tropical cyclone activity, *Geochem. Geophys. Geosyst.*, 9, Q05V03, https://doi.org/10.1029/2007GC001809.

Wang, H., Schubert, S., Suarez, M., and Koster, R. (2010), The physical mechanisms by which the leading patterns of SST variability impact U.S. precipitation, *Journal of Climate*, *23*, 1815-1836.

Wang, S. Y., Hipps, L., Gillies, R. R., & Yoon, J. H. (2014). Probable causes of the abnormal ridge accompanying the 2013-2014 California drought: ENSO precursor and anthropogenic warming footprint. *Geophysical Research Letters*, **41**, 3220–3226. https://doi.org/10.1002/2014GL059748

Watson, S. (2014). Quantifying the variability of wind energy, *WIREs Energy Environ*, **3**, 330–342. https://doi.org/10.1002/wene.95

Weaver, S., Schubert, S., & Wang, H. (2009), Warm season variations in the low-level circulation and precipitation over the central United States in observations, AMIP simulations, and idealized SST experiments, *Journal of Climate*, **22**, 5401–5420, https://doi.org/10.1175/2009JCLI2984.1.

Wiedermann, M., Donges, J. F., Handorf, D., Kurths, J. & Donner, R. V. (2016), Hierarchical structures in Northern Hemispheric extratropical winter ocean–atmosphere interactions. *International Journal of Climatology*, **37**,3821-3836. https://doi.org/10.1002/joc.4956.

Widén, J. (2011). Correlations between large-scale solar and wind power in a future scenario for Sweden. *IEEE Transactions on Sustainable Energy*, **2**, 177–184. https://doi.org/10.1109/TSTE.2010.2101620

Wilks, D.S. (2006). Statistical Methods in the Atmospheric Sciences. 2d ed. International Geophysics Series, Vol. 91, Academic Press, 627 pp.

Xie, P., Yatagai, A., Chen, M., Hayasaka, T., Fukushima, Y., Liu, C., & Yang, S., (2007). A gauge-based analysis of daily precipitation over East Asia. *Journal of Hydrometeorology*., **8**, 607-626. https://doi.org/10.1175/JHM583.1

Xie, P., Chen, M., & Shi, W. (2008). CPC unified gauge-based analysis of global daily precipitation, Western Pacific Geophysics Meeting, Cairns, Australia, 29 July – 1 August, 2008.

Yu, L., Zhong, S., Bian, X., & Heilman, W.E. (2015), Temporal and spatial variability of wind resources in the United States as derived from the Climate Forecast System Reanalysis, *Journal of Climate*, **28**, 1166-1183. https://doi.org/10.1175/JCLI-D-14-00322.1

Zahedi, A. (2011), A review of drivers, benefits, and challenges in integrating renewable energy sources into electricity grid, *Renewable and Sustainable Energy Reviews*, **15**, 4775-4779. https://doi.org/10.1016/j.rser.2011.07.074